CERN-THESIS-2014-255

Charles University in Prague
Faculty of Mathematics and Physics

MASTER THESIS

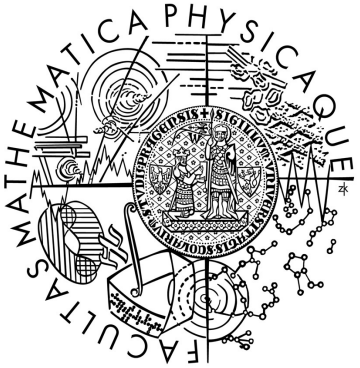

Bc. Michael Pešek

Low temperature polarized target for spin structure studies of nucleons at COMPASS

Department of Low temperature physics

Supervisor of the master thesis: prof. Ing. Miroslav Finger, DrSc.

Study programme: Physics
Specialization: Low temperature physics
Prague 2014

Firstly I would like to thank to my supervisor Miroslav Finger for giving me the opportunity to join the COMPASS experiment and to his support concerning it.

Many thanks belong to whole COMPASS collaboration and especially to the Polarized Target group for their help and for accepting me among them. Special thank belong to Jaakko Koivuniemi for his advices, comments and patience he has with me.

On the personal side – most thanks belong to my longstanding friend Petr Veřtát for his support without which I would never be able to write this thesis. Special thanks belong to Marketa H. for her support on all sides.

I can't also forget to thank the "Czech Mafia at COMPASS" – many thanks to them for their good company and cooking expertise.

And finally I thank to everybody else I forgot to mention here.

I declare that I carried out this master thesis independently, and only with the cited sources, literature and other professional sources.

I understand that my work relates to the rights and obligations under the Act No. 121/2000 Coll., the Copyright Act, as amended, in particular the fact that the Charles University in Prague has the right to conclude a license agreement on the use of this work as a school work pursuant to Section 60 paragraph 1 of the Copyright Act.

In Prague 04. 04. 2014 signature

Název práce: Nízkoteplotní polarizovaný terč pro studium spinové struktury nukleonů v experimentu COMPASS

Autor: Bc. Michael Pešek

Katedra: Katedra fyziky nízkých teplot

Vedoucí diplomové práce: prof. Ing. Miroslav Finger, DrSc.

Abstrakt: V předložené práci je vyložen koncept hlubokého nepružného rozptylu leptonů na nukleonech v kontextu studia spinové struktury nukleonů. Jsou diskutovány nepolarizovaný a polarizovaný případ a je zaveden koncept TMDs (Partonové distribuční funkce závislé na příčné hybnosti). Je popsána možnost meření TMDs za pomoci Semi-inkluzivního hlubokého nepružného rozptylu (SIDIS) společně s příslušnými výsledky získanými na experimentu COMPASS. Je krátce zmíněn budoucí polarizovaný Drell-Yan program na experimentu COMPASS a jeho důležitost vzhledem k testu universality, tj. změny znaménka T-lichých TMDs jsou-li měřeny v Drell-Yan procesu a v SIDIS procesu. Je zdůrazněna důležitost polarizovaného terče pro studium spinové struktury a je vyložen teoretický základ dynamické jaderné polarizace pomocí Solid efektu a konceptu spinové teploty. V detailech je popsán experiment COMPASS s důrazem na polarizovaný terč. Konečně je popsána a provedena procedura kalibrace v tepelné rovnováze a jsou prezentovány její výsledky. Výsledky měření jaderné polarizace za roky 2010 a 2011 jsou prezentovány společně s relaxačními časy. Na závěr jsou diskutovány různé systematické nejistoty.

Klíčová slova: spinová struktura nukleonu, partonová distribuční funkce, dynamická jaderná polarizace, měření jaderné polarizace

Title: Low temperature polarized target for spin structure studies of nucleons at COMPASS

Author: Bc. Michael Pešek

Department: Department of low temperature physics

Supervisor of the master thesis: prof. Ing. Miroslav Finger, DrSc.

Abstract: In presented thesis we describe concept of Deep Inelastic Scattering of leptons on nucleons in context of nucleon spin structure studies. Both polarized and unpolarized cases are discussed and concept of Transverse Momentum Dependent Parton Distribution Functions (TMD PDF) is introduced. The possibility of TMDs measurement using Semi-inclusive DIS (SIDIS) is described along with related results from COMPASS experiment. The future Drell-Yan programme at COMPASS is briefly mentioned and its importance is presented on the universality test i.e. change of sign of T-odd TMDs when measured in Drell-Yan and SIDIS. The importance of Polarized Target (PT) for spin structure studies is highlighted and principles of Dynamic Nuclear Polarization (DNP) are given using both Solid effect and spin temperature concept. COMPASS experiment is described in many details with accent given to PT. Finally the thermal equilibrium (TE) calibration procedure is described and carried out for 2010 and 2011 physics runs at COMPASS. The average polarization measurement results from 2010 and 2011 are presented along with relaxation times. Various uncertainties of the polarization measurement are also discussed.

Keywords: spin structure of nucleon, parton distribution function, dynamic nuclear polarization, nuclear polarization measurement

Contents

Introduction

Since ancient times people has been trying to study and understand structure of world surrounding them. But it took considerable amount of time and development until people were able to reach the level of atoms or to go even deeper in the structure. It all started at the end of 19th century. In 1897 J.J. Thomson discovered electron and then in 1911 E. Rutherford discovered atomic nucleus. In the following decades proton and neutron were discovered. Only in the fifties people reached the level of structure which now seems to be the deepest to exist (famous experiment of Hofstadter at SLAC). Subsequently parton model was born and in seventies the QCD was developed.

It could seem that the story is over. But in 1988 European Muon Collaboration (EMC) discovered that quarks contribute only by one third to the overall spin of a nucleon. This "spin crisis" as it has been labeled has not been solved to these days and it lead to new theoretical development, e.g. the Transverse Momentum Dependent Parton Distribution Functions (TMD PDFs or just TMDs) and to series of successful experiments. One of them is the COMPASS experiment at CERN.

In the following we will describe the details of parton model, the concept of Transverse Momentum Dependent Parton distributions and briefly summarize up to date results obtained by COMPASS to which the results presented here contributed significantly. It will be clear that polarized target is necessary for such studies and details on Dynamic Nuclear Polarization for obtaining the highest degree of target material polarization and polarization measurement (as one of the most important partial results for extracting parton distributions) will be given.

Prospects on new measurements are promising (e.g. Drell-Yan and DVCS measurements in preparation at COMPASS) and we can hope that the spin mystery will be less mysterious before the end of this decade.

1. Physics case – Deep inelastic scattering

In this section we describe the basic ideas of Deep Inelastic Scattering (DIS) of leptons on hadrons and introduce description of hadron structure using so-called Parton Distribution Functions (PDFs). We limit ourselves to the case of nucleon (and mainly considering proton) as target hadron as it is the only stable hadron known and therefore allows for conducting scattering experiments. This part freely follows treatment of the subject presented in [1] and [2]. Later on we introduce concept of so-called Transverse Momentum Dependent PDFs (TMDs) where the transverse momentum of nucleon constituents is also taken into account. Main up to date results are also presented. Natural units $\hbar = c = 1$ are used through the whole section.

1.1 Kinematics of lepton-nucleon scattering and cross-section formula

Let us consider following process of scattering of charged lepton *l* on proton

$$l(k) + proton(P) \rightarrow l(k') + X \ , \tag{1.1}$$

where letters in parenthesess corresponds to four-momenta of given particles and X denotes arbitrary final state hadrons. If *X*=proton then we speak of elastic scattering. This can be described by lowest order Feynman diagrams depicted in fig.1.1. In principle this process can be mediated by photon or by Z boson, but in the fixed target experiments the Z boson contribution can be safely neglected due to collision energy well below Z peak. In case the lepton is neutrino than the process is mediated by $W^{\pm}$ boson but we won't consider this case. The process is usually described by several relativistic invariants, here expressed in terms of both centre-of-mass frame variables and laboratory frame variables (rest frame of proton):

$$s \equiv (k+P)^2 = M^2 + 2\mathrm{k}\cdot P = M(2E_{lab} + M) \tag{1.2}$$

$$Q^2 \equiv -q^2 \equiv -(k-k')^2 = 2\mathrm{k}\cdot k' = 4\mathrm{EE}'\sin^2(\theta_{lab}/2) \tag{1.3}$$

$$y \equiv \frac{q\cdot P}{k\cdot P} = \frac{E_{lab} - E'_{lab}}{E_{lab}} = \frac{\nu}{E_{lab}} \tag{1.4}$$

$$x \equiv \frac{Q^2}{2\mathrm{P}\cdot q} = \frac{Q^2}{2\mathrm{M}\nu} \tag{1.5}$$

$$W^2 \equiv (q+P)^2 = \frac{Q^2(1-x)}{x} + M^2 \ . \tag{1.6}$$

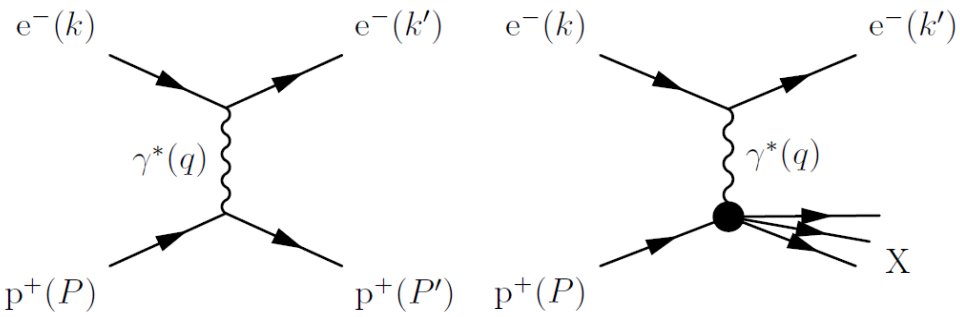

(a) Elastic scattering on pointlike proton

(b) Inelastic scattering

Figure 1.1: Lepton-nucleon scattering in lowest order of Feynman diagrams

The M denotes proton mass, E is energy of scattering lepton, E' is energy of scattered lepton and θ is angle of scattered lepton. The subscript *lab* denotes quantities in laboratory frame. We neglect lepton mass through the whole text. Mandelstam variable s characterizes the initial state as it is total centre-of-mass energy squared. Q^2 is transferred momentum. Precise meaning of x will be shown later in the context of parton model. Here we just mention that x expresses inelasticity of the collision and that x=1 corresponds to elastic scattering which is easily verified.

In unpolarized case the final state lepton is characterized by five variables E'_{lab}, x, y, Q^2 and θ_{lab} of which only two are independent. Commonly x and Q^2 or x and y are used when describing scattering cross-sections.

Finally let us recall (e.g. [3]) the general formula for 1+2 →3+4+... scattering process

$$d\sigma = \frac{(2\pi)^4}{|\vec{v}_1 - \vec{v}_2|} \frac{1}{2E_1} \frac{1}{2E_2} |M_{fi}|^2 \prod_{i=3}^{n} \frac{d\vec{p}_i}{(2\pi)^3 2E_i} \delta^4\left(p_1 + p_2 - \sum_{i=3}^{n} p_i\right) SF \,, \tag{1.7}$$

where M_{fi} is matrix element for considered process E_i is energy of ith particle, p_i is momentum of ith particle, v_1 and v_2 are velocities of initial particles and SF is statistical factor which accounts for identical particles in final state.

1.2 Elastic lepton-proton scattering cross-section

Let us firstly calculate the cross-section for a point-like proton represented by fig.1.1a. The squared spin-averaged matrix element is then given by Feynman rules

$$|\overline{M_{fi}}|^2 = \frac{1}{4} \sum_{spins} \left| \left[\bar{u}(k', s_4) \gamma_\mu u(k, s_2)\right] e^2 \frac{-ig^{\mu\nu}}{q^2} \left[\bar{u}(P', s_3) \gamma_\nu u(P, s_1)\right] \right|^2 , \tag{1.8}$$

where the sum goes over spins of final states and averaging over spins of initial states. (For review of Feynman rules see e.g. [3].) The formula (1.7) yields after straightforward but tedious calculation

$$\frac{d\sigma}{dQ^2}=\frac{2\pi\alpha^2}{Q^4}\left[1+(1-y)^2-\frac{M^2 y}{k\cdot P}\right], \tag{1.9}$$

which after transformation to laboratory system gives

$$\frac{d\sigma}{d\Omega_{lab}}=\sigma_{Mott}\left[1+\frac{Q^2}{2\mathrm{M}^2}\tan^2\left(\frac{\theta_{lab}}{2}\right)\right], \tag{1.10}$$

where σ_{Mott} is the famous Mott scattering formula for scattering of point-like Dirac particle on static electromagnetic field of point charge

$$\sigma_{Mott}=\frac{\alpha^2\cos^2(\theta_{lab}/2)}{4E^2\sin^4(\theta_{lab}/2)}, \tag{1.11}$$

where α is electromagnetic fine structure constant.

If we now consider proton with internal structure we need to modify the point-like coupling in (1.8) to general rank 2 tensor. (Which is in close resemblance to introducing so called formfactors in scattering theory in quantum mechanics, for that see e.g. [4].). Taking into account gauge invariance, Lorentz invariance and parity conservation the most general structure of the modified coupling based on available quantities (that are four momenta of all particles and γ-matrices based structure) is then

$$\bar{u}(P')\left[F_1^{el}(Q^2)\gamma^\mu+\kappa\frac{F_2^{el}(Q^2)}{2\mathrm{M}}i\sigma^{\mu\nu}q_\nu\right]u(P), \tag{1.12}$$

where $\sigma^{\mu\nu}$ is anticommutator of γ -matrices

$$\sigma^{\mu\nu}\equiv\frac{i}{2}[\gamma^\mu\gamma^\nu-\gamma^\nu\gamma^\mu], \tag{1.13}$$

κ is parameter related to magnetic moment of the proton and F_1^{el} and F_2^{el} are elastic electromagnetic formfactors. It is convenient to introduce electric and magnetic formfactors instead of F_1^{el} and F_2^{el}

$$G_E(Q^2)\equiv F_1^{el}(Q^2)-\frac{Q^2}{4\mathrm{M}^2}\kappa F_2^{el}(Q^2) \tag{1.14}$$

$$G_M(Q^2)\equiv F_1^{el}(Q^2)+\kappa F_2^{el}(Q^2). \tag{1.15}$$

The cross-section can be then evaluated similarly to previous case. The result is

$$\frac{d\sigma}{d\Omega_{lab}} = \sigma_{Mott}\frac{E'}{E}\left[\frac{G_E^2 + \tau G_M^2}{1+\tau} + 2\tau G_M^2 \tan^2\left(\frac{\theta_{lab}}{2}\right)\right], \tag{1.16}$$

where new kinematic variable is introduced $\tau \equiv \frac{Q^2}{4M^2}$.

1.3 Deep inelastic lepton-proton scattering cross-section

We now come to description of inelastic scattering. The deep inelastic means that we are in kinematic domain where $Q^2 \gg M^2$ and $\nu \gg M$. Using similar arguments as in elastic case and taking into account that kinetic energy is not conserved (i.e. ν and Q^2 are independent now) the modified coupling leads to cross-section formula (See [1] for detailed derivation.)

$$\frac{d\sigma}{dxdQ^2} = \frac{4\pi\alpha^2}{Q^4}\left[\left(1 - y - \frac{M^2 xy}{s}\right)\frac{F_2(x,Q^2)}{x} + y^2 F_1(x,Q^2)\right], \tag{1.17}$$

or in laboratory frame

$$\frac{d\sigma}{dE'd\Omega_{lab}} = \sigma_{Mott}\left[\frac{F_2(x,Q^2)}{\nu} + \frac{2F_1(x,Q^2)}{M}\tan^2\left(\frac{\theta_{lab}}{2}\right)\right], \tag{1.18}$$

where $F_1(x,Q^2)$ and $F_2(x,Q^2)$ are proton structure functions. (If we recall that variable x expresses inelasticity of the scattering it is possible to restore the formula for elastic case by setting x=1.)

Both elastic formfactors and structure functions were measured for the first time at SLAC laboratory using electron beam. (And later on by other different laboratories using variety of beams and targets.) The experimental results showed rapid decrease of elastic formfactors with rising Q^2 whereas the (inelastic) structure functions seemed to approach constant non-zero value. The rapid decrease of elastic formfactors has simple explanation. If the nucleon has internal structure then it is less likely for the constituents to recombine back at higher energies of colisions. Bjorken predicted that the structure functions really should approach non-zero constant value. This is called Bjorken scaling. (See [5].) In reality the structure functions do approach zero but very slowly, much slower than elastic formfactors, so called approximate scaling. The F_2 structure function has been since then measured in broad range of x and Q^2. The fig.1.2 shows one the most recent results by H1 and

Zeus collaboration at HERA together with results by older experiments from CERN and Fermilab. (See [6].)

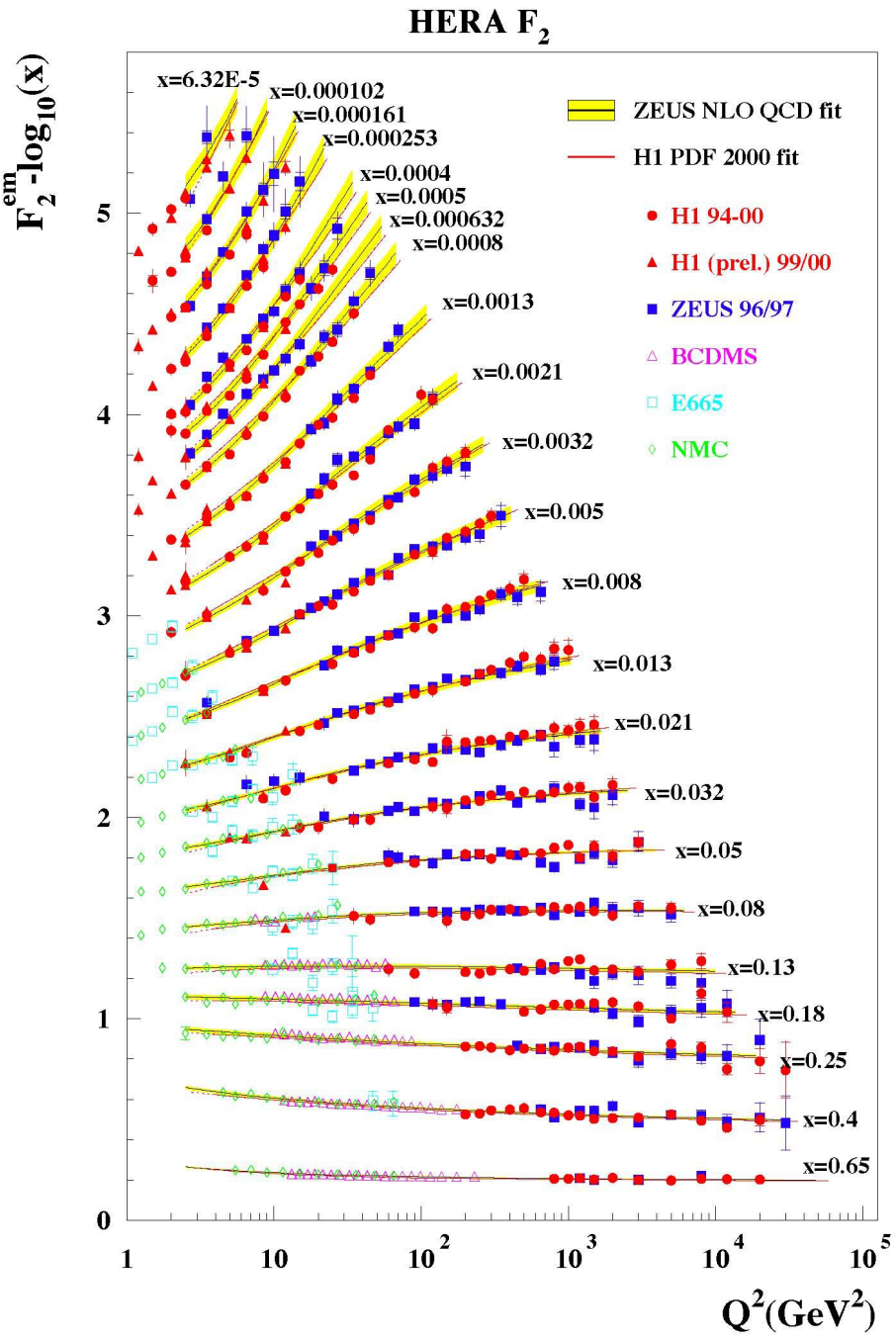

Figure 1.2: $F_2(x,Q^2)$ function measured at HERA, CERN and Fermilab

1.4 Parton model and QCD

It was eventually Feynman who interpreted the results and developed the so called parton model. (Where parton is abbreviation for part of proton.) The main idea is based on the assumption that DIS can be modelled as „quasi-free scattering from

point-like constituents within the proton as viewed from a frame where proton has infinite momentum." (As stated in [7].)

In the infinite momentum frame the transverse momenta of proton constituents as well as their masses can be neglected and parton four-momentum can be then written as $p=\eta P$ that is the fraction the proton four-momentum. If we consider momentum conservation at the proton vertex of fig.1.1a

$$(\eta P')^2=(\eta P)^2-Q^2+2\eta q\cdot P\Rightarrow \eta=\frac{Q^2}{2\mathrm{P}\cdot q}\,, \tag{1.19}$$

then we see that the variable x coincides with η within the parton model.

The lepton-proton scattering cross-section can be now written as incoherent sum of cross-sections from scattering on individual charged partons. To make the model consistent Feynman also added basic mechanism of hadronisation i.e. process of conversion of the partons to final state hadrons. In this description the scattering process takes much shorter time than the hadronisation which occurs much later and does not interfere with it. Considering high energy limit $s\rightarrow\infty$ of (1.17) and noting that in this limit the elastic cross-section on parton with charge fraction e_p is given by

$$\frac{d\sigma}{dQ^2}=\frac{4\pi\alpha^2 e_p^2}{Q^4}\,, \tag{1.20}$$

then the inelastic lepton-proton cross-section can be expressed by comparing (1.17) to weighted sum of (1.20) as

$$\frac{d\sigma}{dxdQ^2}=\frac{4\pi\alpha^2}{Q^4}\frac{F_2(x,Q^2)}{x}=\frac{4\pi\alpha^2}{Q^4}\sum_i e_i^2 f_i(x)\,, \tag{1.21}$$

where $f_i(x)$ is probability to find parton of type i with charge e_i and momentum fraction xP inside the proton. Then the $F_2(x,Q^2)$ can be expressed as

$$F_2(x,Q^2)=F_2(x)=x\sum_i e_i^2 f_i(x)\,. \tag{1.22}$$

The functions $f_i(x)$ are so called Parton Distribution Functions (PDFs). As can be seen the parton model leads naturally to Bjorken scaling. For finite energies the F_1 also plays role in the cross-section. This model implies for ½ spin partons the Callan-Gross relation $F_2(x,Q^2)=2\mathrm{xF}_1(x,Q^2)$ which has been approximately confirmed by data. (See [1].)

It would seem natural to identify the partons with constituent quarks of the additive quark model but this brings some difficulties which prevent this. Considering only u, d, c and s quarks (as the b and t quarks are much heavier than proton) the proton structure function can be written as sum of corresponding PDFs of quarks and antiquarks. (here we denote quark PDFs as $q(x)$ and antiquark PDFs as $\bar{q}(x)$ where q denotes quark flavour.

$$F_2^p(x) = x\left(\frac{4}{9}[u(x)+\bar{u}(x)+c(x)+\bar{c}(x)]+\frac{1}{9}[d(x)+\bar{d}(x)+s(x)+\bar{s}(x)]\right), \qquad (1.23)$$

If we now integrate $F_2^p(x)$ over x we obtain mean square charge per parton. The experimental value ([1]) 0.17±0.009 is clearly inconsistent with expected value of 1/3. This indicates that there must be also electrically neutral partons inside the proton.

The second problem is that the parton distributions behave roughly as 1/x for $x \to 0$ causing their integrals to diverge. This disturbing behaviour means that there is infinite number of charged partons inside the proton. If we now introduce so called valence distributions $q_{val} \equiv q(x) - \bar{q}(x)$ and sea distributions $q_{sea}(x) \equiv \bar{q}(x)$ then it turns out that the valence distributions are integrable and the experimental results for u and d quark gives

$$\int_0^1 dx\, u_{val}(x) \doteq 2 \text{ and } \int_0^1 dx\, d_{val}(x) \doteq 1 \qquad (1.24)$$

which are in agreement of additive quark model.

Another problem is that the integral $\int_0^1 dx\, x \sum_q q(x)$ which represents fraction of momentum carried by quarks has experimental value about 0.5 ([1]) which again indicate presence of uncharged partons.

The above mentioned problem are resolved in full theory of strong interaction called Quantum Chromodynamics (QCD). Formally it is non-abelian gauge field theory based on SU(3) group. They are eight massless vector bosons called gluons (corresponding to eight SU(3) generators) mediating the interaction between quarks which carry color charge. There exist three colour charges R, G and B carried by quarks and corresponding anticolours carried by antiquarks. In contrast to QED the gluons also carry colour charges which allows direct gluon-gluon interaction.

Another significant difference to QED is that the β-function in renormalization group equation is negative leading to running coupling of the interaction which gets weaker with rising energy. That means that in limit of infinite energy the quarks are free. This fenomenon is known as asymptotic freedom and its theoretical discovery brought Gross, Politzer and Wilczek Nobel Prize in 2004. (See [8],[9],[10].) On the other hand in low energy regime (lower than 1 GeV) the coupling is so strong that it does not allow for perturbative treatment and leads to confinement i.e. no free quarks exists. That means that e.g. predicting low energy properties of hadrons and hadronization i.e. formation of hadrons from quarks needs different approach. (E.g. Lattice QCD which discretizes the space-time and uses numerical simulations or chiral perturbation theory which is based on effective lagrangians constructed upon knowledge of QCD symmetries.) The hadronisation is usually described by so-called Fragmentation Functions (FFs) which describe the probability of quark forming given hadron with given momentum.

To summarize the nucleon consists of 3 valence quarks described by valence distributions and are held together by potential formed by multigluon exchange among them. Up to that quark-antiquark pairs are created and annihilated all the time. If they have low enough energy they „live“ long enough to be able to participate in scattering process and their distributions can also be measured. The fig.1.3 shows measured quark and gluon distributions taken from [11].

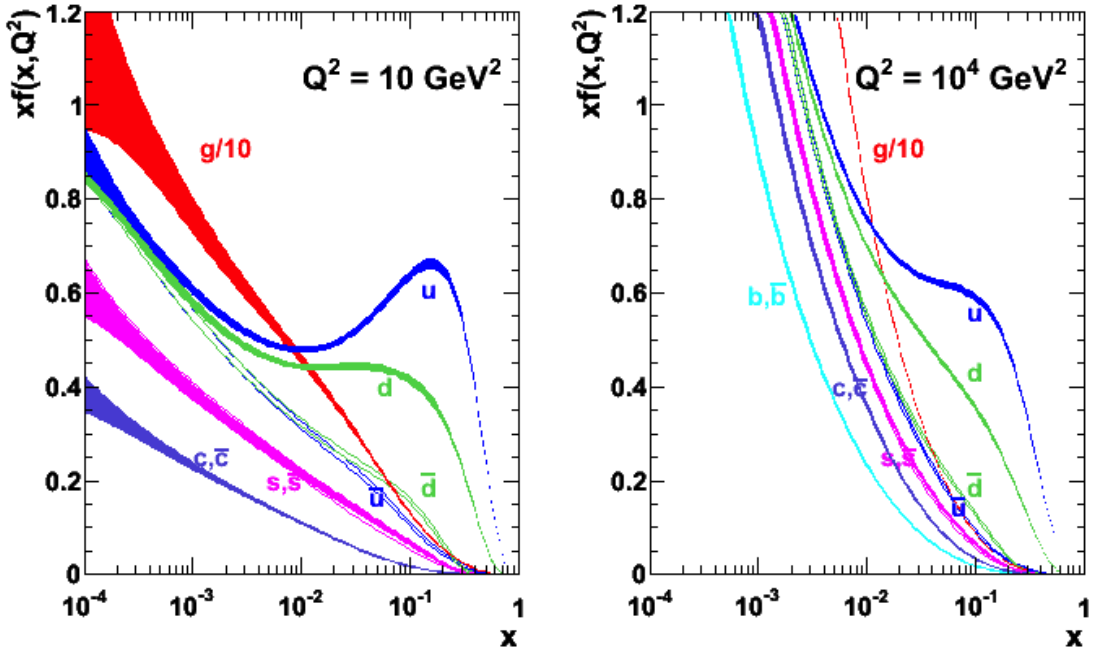

Figure 1.3: Measured parton distribution functions for two values of Q^2

1.4 Polarized case – collinear approximation

We will now consider polarized scattering. If the lepton and nucleon are polarized then the spin four-vector of the nucleon becames another four-vector from which more complex tensor structure of the coupling in (1.12) can be constructed. This imply that at leading order of perturbative QCD in collinear approximation (i.e. neglecting transverse momenta of partons) the nucleon structure can be described by three PDFs (See [12]). These are the previously mentioned unpolarized PDF $q(x) \equiv f_1^q(x)$, the helicity distribution

$$g_1^q(x) \equiv \Delta q \equiv q\uparrow(x) - q\downarrow(x), \tag{1.25}$$

which describes difference between unpolarized PDFs for quarks with spin parallel or antiparallel to the spin of nucleon in case the nucleon is longitudinally polarized and transversity distribution $h_1^q(x) \equiv \Delta_T q$ which describe similar situation but in transversely polarized nucleon. Note that there are two different notations and both of them are commonly used in literature.

The helicity distribution can be measured using polarized lepton beam and longitudinally polarized target. Measuring cross-section for spin of the beam and target parallel and antiparallel following asymmetry can be determined

$$A_1 = \frac{d\sigma^{\uparrow\uparrow} - d\sigma^{\uparrow\downarrow}}{d\sigma^{\uparrow\uparrow} + d\sigma^{\uparrow\downarrow}}. \tag{1.26}$$

Using QED Feynman rules, taking into account high energy limit i.e. neglecting lepton mass, using only helicity instead of full spin four-vector and using parton model we get after some calculation

$$A_1(x) = \frac{(1-(1-y)^2)}{(1+(1-y)^2)} \frac{x}{F_2(x)} \sum_i e_i^2 \Delta q_i. \tag{1.27}$$

This means as long as we know F_2 structure function the helicity distribution can be determined by measurement of the asymmetry (1.26). It should be stressed that meassured asymmetry is smaller by factor $P_T P_B f$, where P_T is target polarization, P_B is beam polarization and f is dilution factor i.e. fraction of polarizable nuclei in the target. (Which is discussed in more detail in section 3.3.) This means that for precise determination of helicity distribution the precise knowledge of beam and target polarization is essential.

If we now consider integrals from helicity distributions

$$\Delta(q) \equiv \int_0^1 dx\, g_1^q \tag{1.28}$$

for different quark flavours the contribution of quarks to proton spin can be then determined. The so called Jaaffe-Manohar sum rule [13] decomposes the spin of the nucleon

$$S = \frac{1}{2}\Delta\Sigma + \Delta G + L_q + L_g, \quad \Delta\Sigma = \Delta(u) + \Delta(d) + \Delta(s) \tag{1.29}$$

where $\Delta\Sigma$ is the quark contribution, ΔG is gluon contribution and L is orbital angular momentum of quarks and gluons. This was firstly measured by EMC collaboration and later by SMC collaboration and by COMPASS colaboration. The recent result obtained by COMPASS ([14]) is $\Delta\Sigma$=0,31±0.03. Firstly measured by EMC ([15]) this has been called „spin crisis“ as the naive expectation that quarks are responsible for major part of proton spin does not hold and it remains unsolved to these days. The gluon contribution has been measured since then by COMPASS.

The transversity distribution is much more difficult to measure and is still rather poorly known despite being leading order quantity. The reason for that is that it is chiral-odd function i.e. it needs chirality flip of concerned quark and probability of such process is strongly suppressed by chirality conservation law in DIS process. It can be however measured in semi-inclusive DIS (i.e. DIS where one of the final state hadron is identified) or in Drell-Yan process (two hadrons in initial state produces two leptons in final state via quark-antiquark annihilation). Both of these processes involve two hadrons and this allows for double chirality flip needed for the measurement (see [12]). We will discuss both of these processes later on.

1.5 Transverse momentum dependent PDFs

If we proceed beyond collinear approximation to next-to-leading order description of the nucleon spin structure we need to take into account the transverse momenta $\vec{k}_T$ of the quarks. This can be done for small transverse momenta (which is the case e.g. at COMPASS) by concept of Transverse Momentum Dependent PDFs (TMDs). In following we use so-called Amsterdam notation ([16]) where *f*, *g* and *h* denote unpolarized, longitudinally polarized and transversely polarized distributions, respectively. The subscript 1 denotes leading order quantity and subscripts T and L

denotes transversely and longitudinally polarized nucleon. Finally the superscript $\perp$ denotes transverse momenta with uncontracted Lorentz indices.

There are in total eight TMDs ([12]) $f_1(x,k_T^2)$, $g_1(x,k_T^2)$, $h_1(x,k_T^2)$, $g_{1\mathrm{T}}^{\perp}(x,k_T^2)$, $h_{1\mathrm{T}}^{\perp}(x,k_T^2)$, $h_{1\mathrm{L}}^{\perp}(x,k_T^2)$, $h_1^{\perp}(x,k_T^2)$, $f_{1\mathrm{T}}^{\perp}(x,k_T^2)$. The first three give unpolarized structure function, helicity and transversity distributions and the other five vanish after integration over k_T^2. The last two functions are T-odd. The Boer-Mulders function $h_1^{\perp}(x,k_T^2)$ describes correlation between the transverse spin and the transverse momentum of the quark in unpolarized nucleon. The Sivers $f_{1\mathrm{T}}^{\perp}(x,k_T^2)$ function describes correlation between the transverse spin of the nucleon and the transverse momentum of the quark. Note that physical motivation for introducing T-odd function is not clear as QCD is T invariant theory (for interested reader we refer to e.g. [12]) but if non-zero they present excellent possibility to test some fundamental properties of QCD e.g. by measurement of polarized Drell-Yan process which will be discussed briefly in section 1.7.

1.6 Semi-inclusive DIS – accessing TMDs

We will now discuss briefly the possibility for experimental study of the TMDs and the transversity function. One of the possibilities is to use so called semi-inclusive DIS (SIDIS) i.e. DIS where on hadron in final state is identified. We consider following process

$$l(k)+proton(P)\rightarrow l(k')+h(P_h)+X\,, \tag{1.28}$$

where *h* is final state hadron and letters in parentheses again denote the four-momenta of given particles. We now introduce two more kinematic variable

$$z=\frac{P\cdot P_h}{P\cdot q}\,,\qquad \gamma=\frac{2\mathrm{M}\,x}{Q}\,, \tag{1.29}$$

where *q* has the same meaning as in section 1.1. i.e. four-momentum of the virtual photon. We consider fully polarized case where λ_e denotes helicity of the beam lepton, $S_\perp$ and $S_\parallel$ denotes transverse and longitudinal spin four-vectors of the target proton with respect to the virtual photon four-momentum. The conversion to the experimentally relevant polarizations with respect to the lepton beam is given by simple change of coordinates and will not be discussed here as it is not relevant for our purposes. Fig.1.4 shows the definition of relevant angles for semi-inclusive DIS.

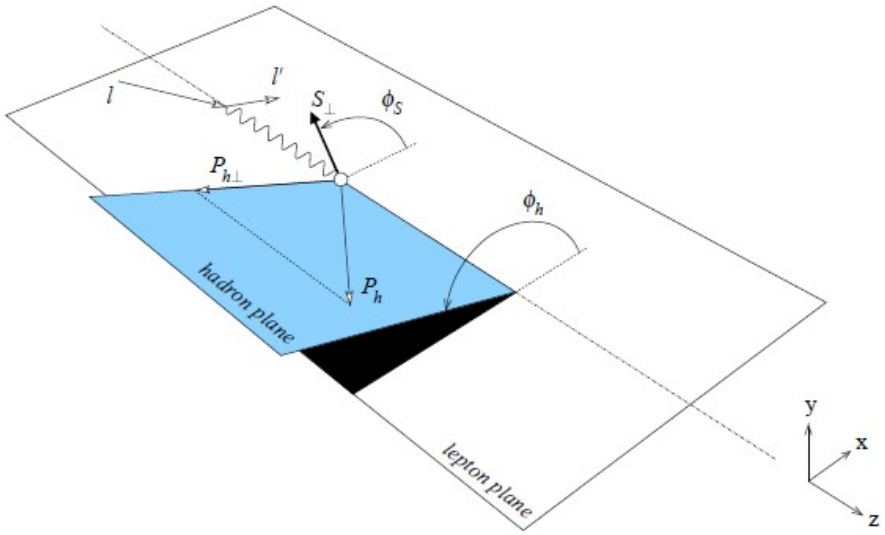

Figure 1.4: Definition of azimuthal angles for semi-inclusive DIS

The general formula for SIDIS cross-section is given by following "master formula" taken from [16]

$$\frac{d\sigma}{dx\,dy\,d\psi\,dz\,d\phi_h\,dP_{h\perp}^2}=\frac{\alpha^2}{xyQ^2}\frac{y^2}{2(1-\epsilon)}\left(1+\frac{\gamma^2}{2x}\right)\Big\{F_{UU,T}+\epsilon F_{UU,L}$$
$$+\sqrt{2\epsilon(1+\epsilon)}\cos\phi_h F_{UU}^{\cos\phi_h}$$
$$+\epsilon\cos(2\phi_h)F_{UU}^{cos2\,\phi_h}+\lambda_e\sqrt{2\epsilon(1-\epsilon)}\sin\phi_h F_{LU}^{\sin\phi_h}$$
$$+S_\parallel\Big[\sqrt{2\epsilon(1+\epsilon)}\sin\phi_h F_{UL}^{\sin\phi_h}+\epsilon\sin(2\phi_h)F_{UL}^{sin2\,\phi_h}\Big]$$
$$+S_\parallel\lambda_e\Big[\sqrt{1-\epsilon^2}F_{LL}+\sqrt{2\epsilon(1-\epsilon)}\cos\phi_h F_{LL}^{\cos\phi_h}\Big] \qquad (1.30)$$
$$+|S_\perp|\Big[\sin(\phi_h-\phi_S)\Big(F_{UT,T}^{\sin(\phi_h-\phi_S)}+\epsilon F_{UT,L}^{\sin(\phi_h-\phi_S)}\Big)$$
$$+\epsilon\sin(\phi_h+\phi_S)F_{UT}^{\sin(\phi_h+\phi_S)}+\epsilon\sin(3\phi_h-\phi_S)F_{UT}^{\sin(3\phi_h-\phi_S)}+\sqrt{2\epsilon(1+\epsilon)}\sin\phi_S F_{UT}^{\sin\phi_S}$$
$$+\sqrt{2\epsilon(1+\epsilon)}\sin(2\phi_h-\phi_S)F_{UT}^{\sin(2\phi_h-\phi_S)}\Big]+|S_\perp|\lambda_e\Big[\sqrt{1-\epsilon^2}\cos(\phi_h-\phi_S)F_{LT}^{\cos(\phi_h-\phi_S)}$$
$$+\sqrt{2\epsilon(1-\epsilon^2)}\cos\phi_S F_{LT}^{\cos\phi_S}+\sqrt{2\epsilon(1-\epsilon^2)}\cos(2\phi_h-\phi_S)F_{LT}^{\cos(2\phi_h-\phi_S)}\Big]\Big\}$$

where x, y, z, γ denotes kinematic variables which have been already introduced, α is electromagnetic fine structure constant and

$$\epsilon = \frac{1 - y - \frac{1}{4}\gamma^2 y^2}{1 - y + \frac{1}{2}y^2 + \frac{1}{4}\gamma^2 y^2}\,. \tag{1.31}$$

The important point here is that the structure functions F are given by convolution of transversity, TMDs and some fragmentation functions. The full list is given in [12]. Therefore in principle it is possible to measure them by measuring the cross-section or more precisely the asymmetries i.e. difference of cross-sections for opposite spin orientations which basically leads to change of normalization of all terms and cancelation of the systematics. The determination of TMDs itself is rather difficult as it requires knowledge of fragmentation functions as deconvolution of fragmentation function from structure functions F is needed to determine TMDs. The fragmentation functions can be precisely measured at lepton colliders where the hadronic final state is given only by FF as there is no structure in the initial state. Interested reader is again referred to literature [16] and [17].

1.7 Polarized Drell-Yan process

In this section we very briefly discuss the polarized Drell-Yan process as COMPASS will be the first experiment in the world to measure it [18] and we show how it can verify some fundamental prediction of QCD. We consider following process

$$H_a(P_a) + H_b(P_b) \rightarrow l^+(k) + l^-(k') + X\,, \tag{1.32}$$

where H_a and H_b denote initial state hadrons and l^+ and l^- denotes final state leptons. The process can be described by Feynman diagram shown in fig.1.5. The process involves a quark from one initial hadron and a anti-quark of the same flavour from second hadron which annihilate to lepton pair.

As we already mentioned in the previous section the SIDIS cross-section is given by the structure functions which are convolution of the TMDs and the FFs. In the case of Drell-Yan process the cross-section is given by convolution of the TMDs of the initial state hadrons only as the final state is leptonic. The QCD predicts that the T-odd TMDs should change their sign when measured in Drell-Yan with respect to those measured in SIDIS i.e.

$f_{1\mathrm{T}}^{\perp}(x, k_T^2)_{Drell-Yan} = -f_{1\mathrm{T}}^{\perp}(x, k_T^2)_{SIDIS}$ and $h_1^{\perp}(x, k_T^2)_{Drell-Yan} = -h_1^{\perp}(x, k_T^2)_{SIDIS}$.

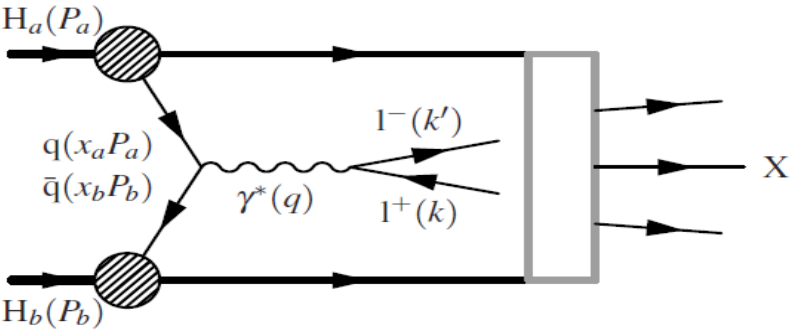

Figure 1.5: Drell-Yan process.

The Drell-Yan process will be realized at COMPASS using pion beam and polarized ammonia target. It has unfortunately rather low cross-section which requires as high intesity of the beam as possible. This brings many experimental difficulties. These are extensively discussed in [18] and [19].

1.8 Short overview of experimental results from COMPASS

To conclude the first part we now give overview of some of the most important results from COMPASS to illustrate the above mentioned theoretical results. The first result shown is A_1 asymmetry for proton from 2007 and 2011 COMPASS runs in fig.1.6. ([20])

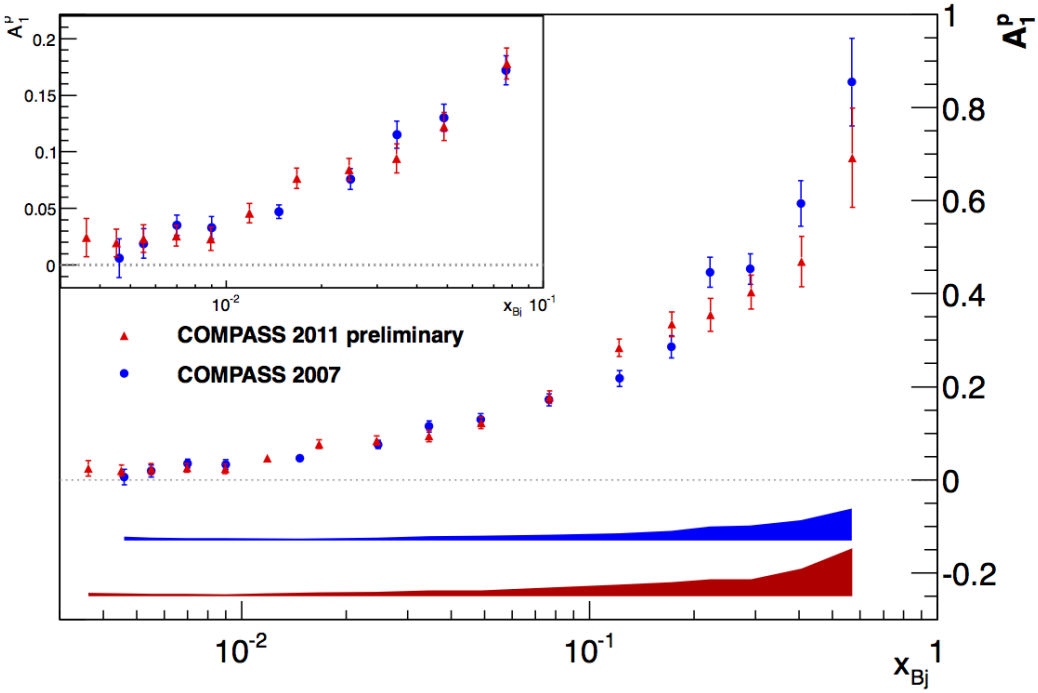

Figure 1.6: A_1 asymmetry for proton, the error bars show statistical uncertainity and the colour stripes show systematics

Next we show results on Collins (fig.1.7) and Sivers (fig.1.8) asymmetries which are related to the transversity and the Sivers function. Note that the Collins asymmetry is convolution of the transversity and the so-called Collins spin-dependent FF which has not been discussed here. For details see [21]. Both were measured independently for positive and negative final state hadron and are presented in bins of x, z and $P_{h\perp}$ in fig.1.7. (See [22] for COMPASS release note.)

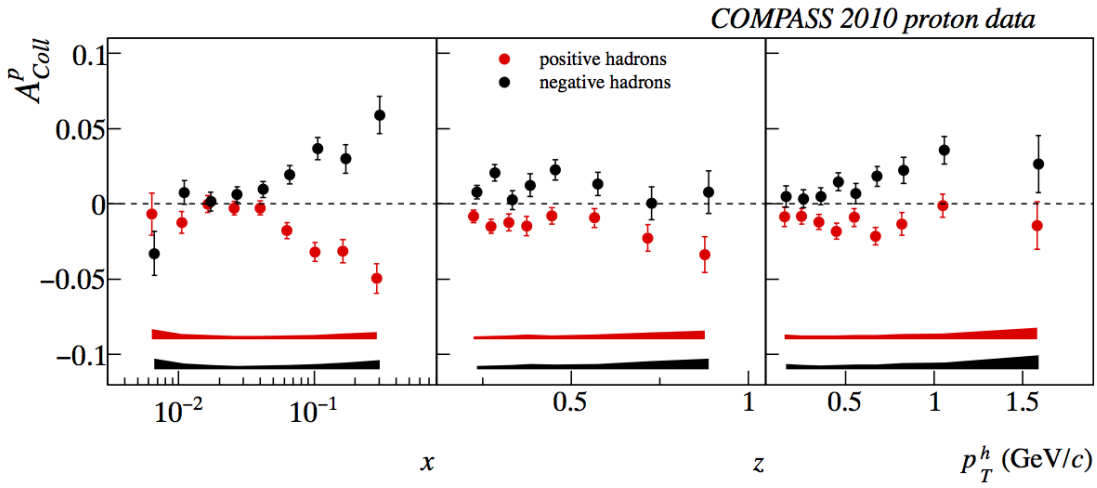

Figure 1.7: Collins asymmetry on proton for both positive and negative hadron

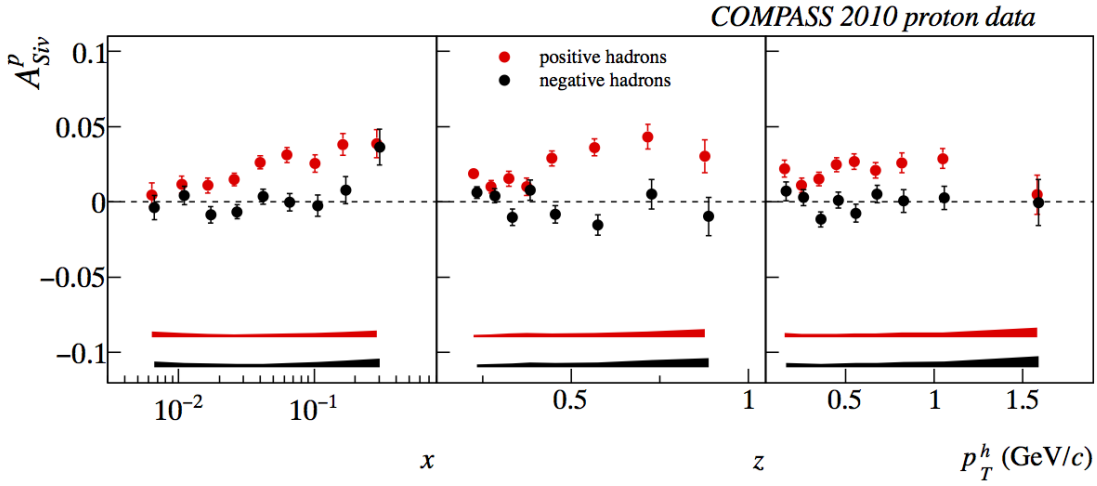

Figure 1.8: Sivers asymmetry on proton for both positive and negative hadron

As can be seen both are clearly non-zero for positive hadrons in x dependence. The Sivers asymmetry result is especially important because it shows that T-odd Sivers TMD is really non-zero.

2. Dynamic Nuclear Polarization

As was shown in previous section obtaining target material with high degree of polarization is crucial for measurement of spin dependent PDFs. There are two widely used methods, namely "brute-force" method and dynamic nuclear polarization (DNP). We will now describe both of these on theoretical grounds.

Consider a system of atoms with nuclei that have non-zero spin *I*. If this system is put into magnetic field B the Zeeman splitting to 2I+1 levels will occur. Hamiltonian of this interaction is given by formula

$$H_{IZ} = -\vec{\mu} \cdot \vec{B} \tag{2.1}$$

where $\vec{\mu} = \hbar \gamma_N \vec{I}$ is magnetic moment corresponding to spin *I,* γ_N is the gyromagnetic ratio. The polarization of the system for spins *I*=1/2 can be expressed as

$$P = \frac{n^+ - n^-}{n^+ + n^-}, \tag{2.2}$$

where n^+ is population of level corresponding to parallel orientation to the magnetic field and n^- to antiparallel orientation. The population of the levels at thermal equilibrium at temperature *T* is given by Boltzmann distribution i.e. density matrix of the system is

$$\rho = \exp(-\beta H_{ZI}) \left[Tr[\exp(-\beta H_{ZI})] \right]^{-1} \tag{2.3}$$

where $\beta = 1/(k_B T)$ is inverse temperature, k_B is Boltzmann constant. The expectation value of the polarization is then given by

$$\langle P \rangle = Tr(\rho P), \tag{2.4}$$

which leads to

$$\langle P \rangle = \tanh(\beta \hbar \gamma IB). \tag{2.5}$$

This formula gives for protons (e.g. ^{1}H in NH_3) in the field of 2.5 T and temperature 1 K net polarization about 0.25 %, for 8 T and 10 mK it gives about 70 % polarization, which is already reasonable value for measurement but the conditions needed are not easily obtained and moreover the thermal relaxation between nuclear system and lattice is extremely slow for insulators i.e. it would take considerable amount of time to reach it. On the other hand this "brute-force" method is usable for metals where the relaxation is much faster. It should be mentioned that for electrons

the polarization is very close to 100 % in moderate conditions (e.g. P = 99.75 % at 2.5 T and 0.5 K).

The basic idea of the DNP is to transfer the high electron polarization to the nuclear system. The following section is freely based on [23] and [24] where the interested reader can find much more details. In the following we denote ω_N the nuclear Larmor frequency of spins I and ω_e the electron Larmor frequency of spins S in external field B, where the Larmor frequency is defined

$$\omega = \gamma B \,, \tag{2.6}$$

where γ is corresponding gyromagnetic ratio.

2.1 Solid effect

Let us first consider assembly of nuclear spins I and electronic spins S in magnetic field. Nuclei are considered spin ½ (e.g. ^{1}H in NH_3). The system can be then described by following hamiltonian

$$H = H_{ZI} + H_{ZS} + H_{II} + H_{SS} + H_{IS} + H_{RF} \,, \tag{2.7}$$

where the terms are in a row nuclear Zeeman interaction, electron Zeeman interaction, nuclear dipolar interaction, electron dipolar interaction, electron-nucleus dipolar interaction and interaction with possible external radiofrequency field. We now consider only one electron-nucleus pair and consider only simple dipolar interaction

$$H_{IS} = \frac{\hbar^2 \gamma_N \gamma_e}{r^3}\left[\vec{I}\cdot\vec{S} - \frac{3(\vec{I}\cdot\vec{r})(\vec{S}\cdot\vec{r})}{r^2}\right], \tag{2.8}$$

where $\vec{r}$ is vector which gives the position of the electron spin S with respect to nuclear spin I. Without dipolar interaction the Zeeman splitting creates four pure states $|{+}{+}\rangle$, $|{+}{-}\rangle$, $|{-}{+}\rangle$ and $|{-}{-}\rangle$, where the + denotes spin oriented in paralel with respect to the magnetic field and − antiparallel to the field. The dipolar interaction can be then treated as perturbation which scrambles the state to perturbed ones $|a\rangle$, $|b\rangle$, $|c\rangle$, $|d\rangle$. The mixing coefficients are given by first order perturbation theory [23]

$$q = \frac{3}{4}\frac{\hbar^2 \gamma_N \gamma_e}{r^3 \omega_N}\sin\theta\cos\theta e^{i\varphi} \,, \tag{2.9}$$

$$p = \sqrt{1 - qq^*}\,, \tag{2.10}$$

where r, θ and φ are spherical coordinates corresponding to vector $\vec{r}$.

The fig.2.1 shows the scheme of the energy levels of the electron-nucleus pair. For the magnetic field at the order of few Tesla and r at the order of few Angstroms the q at the order of 10^{-2}.

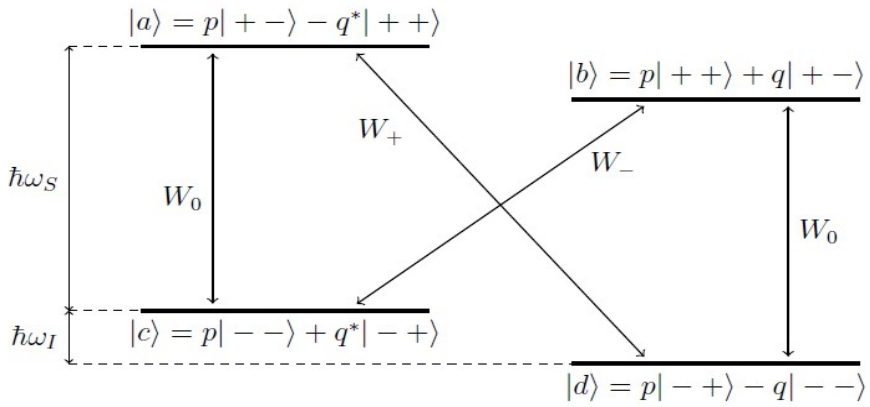

Figure 2.1: Energy levels of electron-nucleus pair paired by dipolar interaction

As can be seen the interaction allows for simultaneous flip of spin S and spin I if the system is irradiated by RF field of frequency $\omega_e \pm \omega_N$ which supplies the energy needed for the transition between corresponding levels. It can be shown that the transition probability is proportional to $|q|^2$ (see [24]).

Then the basic idea of the solid effect is as follows: If a sample in static magnetic field is irradiated by rf field of given frequency the mutual flip-flops of both the electron and nucleus spin occurs. The electron spins relax back during much shorter time than the nuclei, which means that it can induce another flip-flop with other nuclei which then leads to build-up of nuclear polarization. As the probability is proportional to r^{-6} the build-up would be very slow for small concentration (i.e. we can neglect the interaction between them) of paramagnetic impurities (i.e. unpaired electrons, introduced by chemical dopping or by irradiation of the sample) considered here. Fortunately the effect of "spin-diffusion" i.e. energy-conserving flip-flop between nuclei saves the situation.

The above described mechanism has unfortunately several shortcomings. The description described above works only if the width of ESR (Electron Spin

Resonance) line is much smaller then the nuclear Larmor frequency i.e. $\Delta\omega_e \ll \omega_N$. Then it is possible to tune the frequency of the RF field precisely to one of the two frequencies $\omega_e \pm \omega_N$ and induce the transitions in only one direction. This is called "resolved solid effect." If this is not the case than we can speak about "differential solid effect" if the ESR line can be viewed as set of independent spin packets with slightly different Larmor frequencies. This is unfortunately rarely satisfied. Moreover the polarization enhancement calculated by this approach is in disagreement with experiment (see [23]).

It should be stressed that in most materials the condition $\Delta\omega_e \ll \omega_N$ is violated at any value of external field due to inhomogeneous broadening of the ESR line caused by different chemical neighbourhood of the electron spins and the above description of DNP by "resolved solid effect" is not valid.

2.2 Basics of spin temperature theory

The spin temperature theory assumes that the system of electron spins S can be considered isolated and it evolves toward equilibrium which is described by density matrix and (electron) spin temperature T_e (corresponding to inverse temperature β_e). This assumption is valid only when the spin-spin relaxation time of the electron system T_{2e} needed to reach equilibrium among the electron spins is much shorter than the spin-lattice relaxation time T_{1e}. This then implies that the temperature T_e is different from temperature T of the lattice for the time T_{1e}. This means that the spin-lattice relaxation can be understood as equalization of the electron spin temperature T_e and lattice temperature T (see [23]). As the spectrum of the electron spin system has upper limit the temperature T_e can be both positive or negative. The negative temperature then means that the higher levels are more populated than the lower ones and the the entropy of the system decreases wheat heat is transffered to it.

The electron spin-spin reservoir is thermally connected to the nuclear Zeeman reservoir via dipolar interaction. The DNP can be then understood as cooling (in the sense of lowering $|T|$) of the spin-spin reservoir which then results in cooling of the nuclear Zeeman reservoir. The cooling of the nuclear Zeeman reservoir means polarizing nuclear spins, where approaching to the zero temperature from negative temperature means negative polarization and approaching the zero from positive temperatures means positive polarization.

We now proceed to more formal description. We consider the system of electron spins in high magnetic field. The Hamiltonian is then sum of the Zeeman term and the spin-spin term where we assume dipolar interaction

$$H = H_{SZ} + H_{SS} = \sum_i \omega_e S_{zi} + H_{SS} \tag{2.11}$$

where only secular part is taken into account according to first order of perturbation theory

$$H'_{SS} = \frac{1}{2} \sum_{i,j} A_{ij} \left[2S_{zi} S_{zj} - \frac{1}{2} \left(S_{+i} S_{-j} + S_{-i} S_j \right) \right], \tag{2.12}$$

$$A_{ij} = \frac{1}{2} \frac{\gamma_e^2 \hbar}{r_{ij}^{-3}} \left(1 - 3\cos^2 \theta_{ij} \right). \tag{2.13}$$

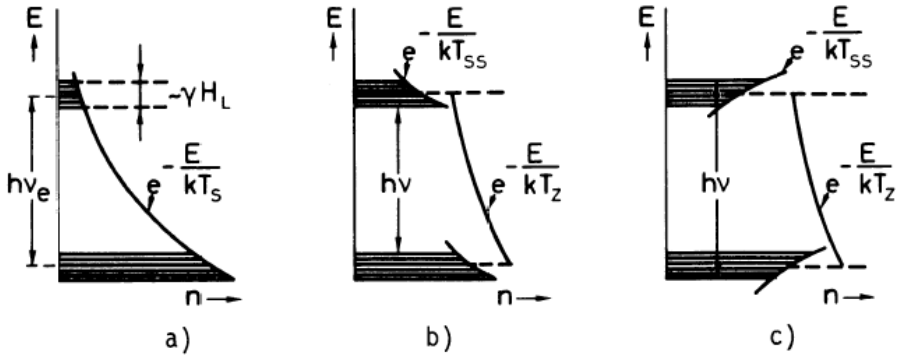

Figure 2.2: Population of the energy levels for spins in high magnetic field: a) in thermal equilibrium b,c) after irradiation by RF field with frequency v (slightly different from Larmor frequency v_e) T_Z and T_{SS} denotes Zeeman temperature and the temperature of the electron spin-spin reservoir respectively (figure taken from [24])

The broadening of the levels (due to spin-spin interaction) in high magnetic field is much smaller than then distance between the levels. This is shown in fig.2.2. Apart from the total energy $\langle H \rangle$ also the Zeeman energy $\langle H_{SZ} \rangle$ is conserved as the internal processes must conserve energy and the change of Zeeman energy cannot be compensated by change of spin-spin energy i.e. if there is spin flipped down then there must be another one which is flipped up. This means that the spin-spin energy $\langle H_{SZ} \rangle$ is also conserved and density matrix can be then written (see [23]) as

$$\rho = \exp\left(-\alpha \omega_e S_z - \beta_e H'_{SS} \right) \left\{ Tr\left[\exp\left(-\alpha \omega_e S_z - \beta_e H'_{SS} \right) \right] \right\}^{-1}, \tag{2.14}$$

where α is inverse temperature of the Zeeman reservoir and β_e is the inverse

temperature of the spin-spin reservoir. If we now consider two levels a and b separated by energy $\hbar(\omega_e-\Delta)$, $|\Delta|\ll\omega_e$ then the ratio of their population is

$$\frac{p_a}{p_b}=\exp(\alpha\omega_e-\beta_e\Delta)\,. \tag{2.15}$$

If the material is now irradiated by rf field with frequency $\omega_e-\Delta$ the populations of the levels can be equalized (if we neglect the spin-lattice relaxation) which implies

$$\alpha\omega_e=\beta_e\Delta\,, \tag{2.16}$$

i.e. the absolute value of the spin temperature $|T_e|$ can be much lower then the lattice temperature $|T|$ and we see that for $\Delta<0$ we obtain negative temperature which corresponds to fig.2.2c). If we now change the reference frame to the one rotating at frequency $\omega_e-\Delta$ perpendicular to the external field *B* the hamiltonian (2.11) changes to effective one

$$H_{eff}=S_z\Delta+H'_{SS}+S_x\omega_1\,, \tag{2.17}$$

where ω_1 is Larmor frequency corresponding to the RF field. The Zeeman temperature α then changes to $\alpha'=\alpha\omega_e/\Delta$ so the eq. (2.16) changes to $\alpha'=\beta_e$ in the rotating frame.

If we now assume high temperature limit (i.e. the energy of one spin is much smaller than thermal energy k_BT_e) the rate equations for α', β_e can be derived (see [23]). After addition of the relaxation terms (responsible for spin-lattice relaxation) the so-called Provotorov equations then read

$$\begin{aligned}\frac{d\alpha'}{dt}&=-W(\alpha'-\beta_e)-\frac{\alpha'-\alpha_L}{T_{1Z}}\\ \frac{d\beta_e}{dt}&=W\frac{\Delta^2}{D^2}(\alpha'-\beta_e)-\frac{\beta_e-\beta_L}{T_{1D}}\end{aligned}\,, \tag{2.18}$$

where $W=\pi\omega_1^2 g(\Delta)$ with $g(\Delta)$ being the NMR absorption lineshape and

$$D=\gamma_e B'_{loc}=\sqrt{Tr(H'^2_{SS})[Tr(S_z^2)]^{-1}}\,, \tag{2.19}$$

is the local Larmor frequency in the rotating frame. The subscript L denotes values at equilibrium with lattice and β_L denotes lattice inverse temperature.

If we now consider the case with no RF field the polarization and spin-spin energy now evolve according to

$$\frac{d}{dt}\langle S_z\rangle_{relax} = -\frac{\langle S_z\rangle - \langle S_z\rangle_L}{T_{1Z}}$$
$$\frac{d}{dt}\langle H'_{SS}\rangle_{relax} = -\frac{\langle H'_{SS}\rangle - \langle H'_{SS}\rangle_L}{T_{1D}}, \quad (2.20)$$

where T_{1Z} denotes "Zeeman-lattice" relaxation time and T_{1D} the "spin-spin-lattice" relaxation time. The steady temperatures can be now calculated from these equations. In limit of strong field we get

$$\beta_e^{eq} = \beta_L \frac{\omega_e \Delta}{\Delta^2 + (T_{1Z}/T_{1D}) D^2}. \quad (2.21)$$

In case of DNP when the spin-spin reservoir is thermally connected to nuclear Zeeman reservoir the results needs to be modified (see[23])

$$\beta_e^{eq} = \beta_L \frac{\omega_e \Delta}{\Delta^2 + (T_{1Z}/T_{1D}) D^2 (1-f)}, \quad (2.22)$$

where f is so-called leakage factor which takes into account the relaxation of nuclear spins through dipolar interaction with electron spins.

The results of the spin temperature theory can be illustrated in case when two different types of nuclear spins are present. The SMC collaboration (see [25]) performed DNP on HN_3 and measured independently the polarization of both ^1H and ^{14}N during the process. The spin temperature was found to be equal. This result was latter used at COMPASS to determine the nitrogen polarization without it direct measurement. (See Section 4.)

3. COMPASS experiment at CERN

COMPASS (Common Muon and Proton Apparatus for Structure and Spectroscopy) is fixed target experiment located in North Area at CERN Prevessin site. Approved in 1997 COMPAS started data taking in 2002. In 2005 during accelerator shutdown, COMPASS underwent some modification to its setup – namely new polarized target magnet with larger acceptance and RichWall detector were installed. COMPASS phase II was approved in 2010 and started in 2012 by run dedicated to Primakoff measurements (to measure charged pion polarizabilities and verify χPT predictions) and "dress rehearsal" for DVCS measurement. At the end of 2014 and during 2015 COMPASS will measure polarized Drell-Yan process which will be followed by two years of DVCS measurement. Proposal is being prepared for next stage of measurements after 2017 (another year of Drell-Yan measurement, possibly polarized DVCS and more un/polarized deep inelastic scattering)

In following section we describe in more details the M2 beamline for the experiment, setup of the spectrometer with details of the most important detectors and polarized target. (All numbers are taken from [26].)

3.1 Beamline

COMPASS uses secondary hadron or tertiary muon beam from SPS accelerator. The proton beam from SPS is extracted on T6 beryllium target during so-called spill, which lasts (depending on SPS setup) between 8 to 10 seconds. Spill is followed by longer period without beam on T6, which is mostly around 30 to 40 seconds. The spill period plus no beam period put together is called supercycle.

Proton beam impacting on T6 produces secondary hadron beam which can have momentum between 120 GeV/c to 280 GeV/c and can be directly send through the M2 beamline. The momentum is simply selected by setting the bending magnets current. By the same means the sign of charge of the particles can be selected too.

The beamline itself consists mostly of bending dipole magnets and focusing quadrupole magnets and beam position monitoring based on scintilating detectors. Overall length of the beamline is about 1 km.

COMPASS has two differential Cherenkov detectors (called CEDARs) available for identification of particles contained in the hadron beam. The beam consists

approximately of 97 % of pions, 2.3 % of kaons and the rest are antiprotons and other particles.

Another possibility is to use hadron absorber (called TAX) which stops completely the hadron beam and allows only muons from pion decays to come through. The muon beam can have momentum between 80 GeV/c to 200 GeV/c and the muons are naturally polarized due to V-A character of weak interaction responsible for charged pion decay. The polarization has been measured to be -80±4 %. (See [26].) For the use of the muon beam the last section of the beamline contains six so-called Beam Momentum Stations (BMS), which can be moved in and out of the beam and serve for precise determination of muon beam momentum.

3.2 Spectrometer

COMPASS spectrometer consists of three parts - the target (which can be both polarized and unpolarized) and the so called Large Angle Spectrometer (LAS) and Small Angle Spectrometer (SAS). Layout of COMPASS (taken from [26]) used during run 2010 (very similar setup was used during 2011) is shown in fig. 3.1. The setup is designed to have large angular and momentum acceptance.

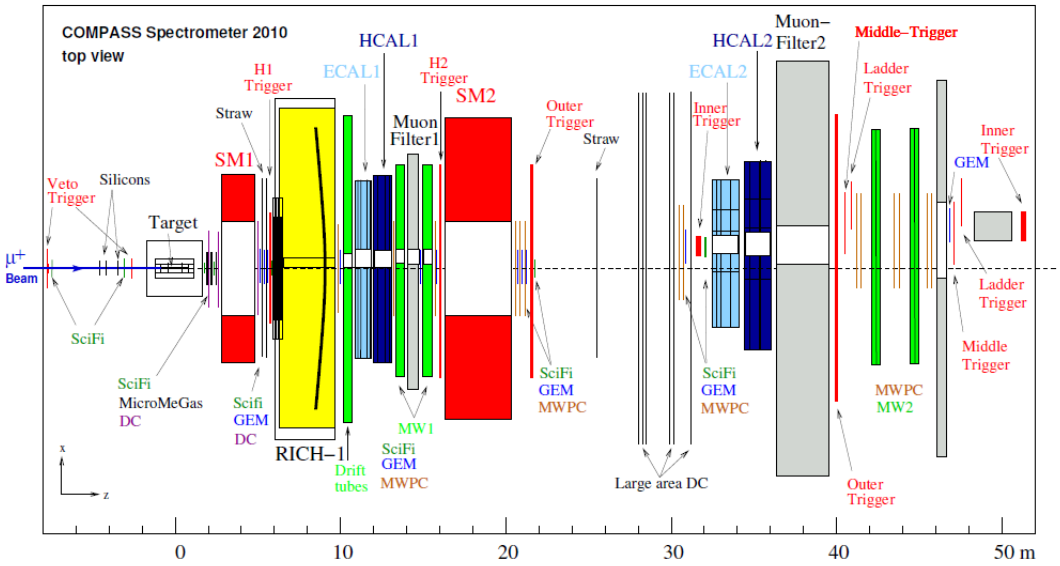

Figure 3.1: COMPASS setup in 2010

Both LAS and SAS are based on strong dipole magnets with large aperture (called SM1 and SM2 respectively) and both are equipped by electromagnetic and hadronic calorimeters and several dozens of tracking planes of various types

depending on its position with respect to the beam. LAS is moreover equipped by Ring Imaging Cherenkov Detector (RICH) for particle identification. The crucial part of the whole setup is also the trigger and the DAQ (Data Acqusition System). We describe details of individual detectors and systems in the following section.

3.2.1 Tracking system

The tracking system is crucial part of the setup as tracking of the charged particles bended in magnetic field provides information needed to determine their momentum. It consists of several different types of detector of different sizes according to its position with respect to the beam and the target. The more closer to target the more space resolution is needed. First part of the tracking is **Beam telescope** which precisely determines the tracks of incoming beam particles. It consists of so-called **SciFi** (scintillating fibres) detectors and the **silicon detectors**. Both have to cope with extremely high particle flux and have to have excellent spatial resolution better than 50 μm. The SciFi detector consists of about 8000 scintillating fibres glued together and which are read out by 2500 photomultipliers. These have excellent time resolution of 0.4 ns which is used for track reconstruction rather than spatial resolution. The microstrip silicon detectors have spatial resolution of about 10 μm and their front-end electronics is cooled by cool nitrogen gas to lower the noise. Both of these detectors form so-called very small area trackers.

The small area trackers are used to track particle in close distance from the beam through out the spectrometer. Again high spatial resolution is needed. They are realized by so-called Micromesh gaseous structure detectors (**Micromegas**) and Gaseous electron multiplier (**GEM**) detectors. Both have spatial resolution between 70 μm to 90 μm. The Micromegas (based on wire chamber design and developed by Charpak's group in Saclay [27] in 1990s) have three electrodes. When a particle hits the detector it ionizes the gas. The produced electrons then drifts toward mesh electrode with high voltage which serves as amplifier of the signal producing avalanche which is then detected by strips behind. The amplification gap between strips and mesh is very narrow – about 100 μm which allows for fast response of the detector – less than 1 ns. The scheme is shown in fig.3.2a. The detector station consists of four detection planes and the active area is 40x40 cm^2 and has a 5x5 cm^2 dead area at the centre where the beam comes through. The GEM (developed in 1997 at CERN [28]) detector stations are composed of two planes and have active area of

31x31 cm^2. They have two main electrodes and three isolating layers with metal foil with high voltage on both sides to amplify the ionisation signal from passing particle. Its scheme is shown in fig. 3.2b.

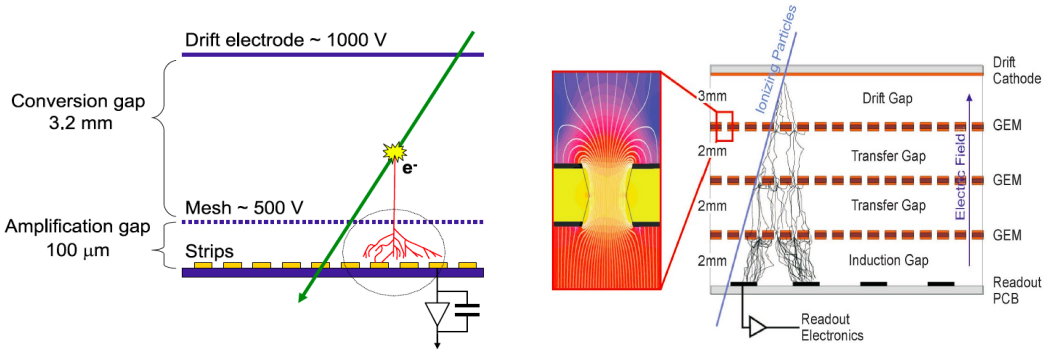

a) Micromegas b) GEM

Figure 3.2: Schemes of Micromegas and GEM detectors

For large area tracking **Drift chambers** (DC), **Straw tube detectors** and **Multiwire proportional chambers** (MWPC) are used. They have moderate spatial resolution ranging from 200 μm for DC to 1.6 mm for MWPC. Active area of the DC is 180x127 cm^2 for LAS and 500x250 cm for SAS. The MWPC have dimensions 178x120 cm^2 and Straws have dimensions of 323x280 cm^2. The all have dead zone in the centre approximately 20x20 cm^2 to prevent saturation of detector by non-interacting beam flux. The Straws detector consists of plastic tubes in two layers coated with metallic cathode and a anode wire in the center functioning like ionization chamber.

The magnetic field for measurement of particle momentum is provided by two normal-conducting magnet in both LAS and SAS stages of the spectrometer. It is **SM1** dipole magnet in LAS with field integral of 1.0 Tm and with aperture 229x152 cm^2 which matches the target magnet acceptance of 180 mrad and **SM2** magnet in SAS with aperture 2x1 m^2 and field integral of 4.4 Tm. The SM2 is powered by 600 V and 5000 A which gives impressive power input of 3 MW. Both magnets are water cooled.

3.2.2 Calorimetry

COMPASS currently has two electromagnetic (ECAL1 and ECAL2) and two hadronic calorimeters (HCAL1 and HCAL2). Each of type in each stage. New

electromagnetic calorimeter ECAL0 is currently being built for Deeply virtual compton scattering measurement in 2016-2017.

The ECALs are mostly homogenic calorimeters i.e. the calorimeter modules are in one piece which serves both as absorber and scintillator. The modules are made of lead glass and are read out by photomultipliers. Most of the modules are reused ones from GAMS-4000 spectrometer with dimensions 38x38 mm^2. There are about 3000 of them in the central part of ECAL1 and these are supplemented by peripheral Olga modules with dimensions 14.3x14.3 cm^2. The most central part of ECAL2 consists of shashlik-type modules which are then supplemented by radiation hardened GAMS modules (due to larger particle flux) and larger Mainz modules 75x75 mm^2. The shashlik-type modules are sampling calorimeter i.e. alternating layers of absorbers and scintillators. Both calorimeters have central hole to allow passing of non-interacting beam and particles scattered in small angles in case of ECAL1.

The HCALs are both sampling shashlik-type calorimeters. There are 480 modules forming HCAL1 with thickness of 4.8 interaction lengths. HCAL2 has in total 218 modules. All modules are read out by photomultipliers and small portion of the signal can be used in trigger electronics. Both calorimeters have LED system for stability monitoring during data taking. The light of single LED is distributed to all modules by optical fibres. The energy resolution of HCAL1 was measured to be $\sigma(E)/E = 59.4\%/\sqrt{E} \oplus 7.6\%$ and the energy resolution of HCAL2 to be $\sigma(E)/E = 66\%/\sqrt{E} \oplus 5\%$ for energy in units of GeV.

3.2.3 RICH detector

The RICH detector is used for identification of charged hadrons with momenta between 1 GeV/c to 43 GeV/c. It is based on the Cherenkov effect i.e. emission of electromagnetic radiation when charged particle is passing through dielectric medium with velocity greater than phase velocity of light in that medium. The detector itself consists of three main parts, namely vessel with active medium, reflective surface and photodetectors. The scheme of the detector is presented in fig. 3.3. It uses C_4F_{10} gas at pressure of 1 Pa as the active medium. It has volume about 80 m^3. For ensuring the transparency of the medium which is essential the gas is purified regurarly. The reflective part consists of two mosaic spherical mirrors

consisting of 116 hexagonal and pentagonal mirrors. The total reflective area is about 21 m^2.

The photo detection is currently based on MWPC detectors equipped with CsI photocathodes. The Cherenkov light is converted by the photocathode and the produced photoelectrons are amplified by the MWPC. The central part is equipped by fast multi-anode photomultipliers. There is currently extensive R&D ongoing to produce relatively cheap (with respect to photomultipliers) and much superior detectors based on ThGEM technology (i.e. GEM where the thin isolating layer is replaced by more robust printed circuit board, see [29]) to replace the rest of the system.

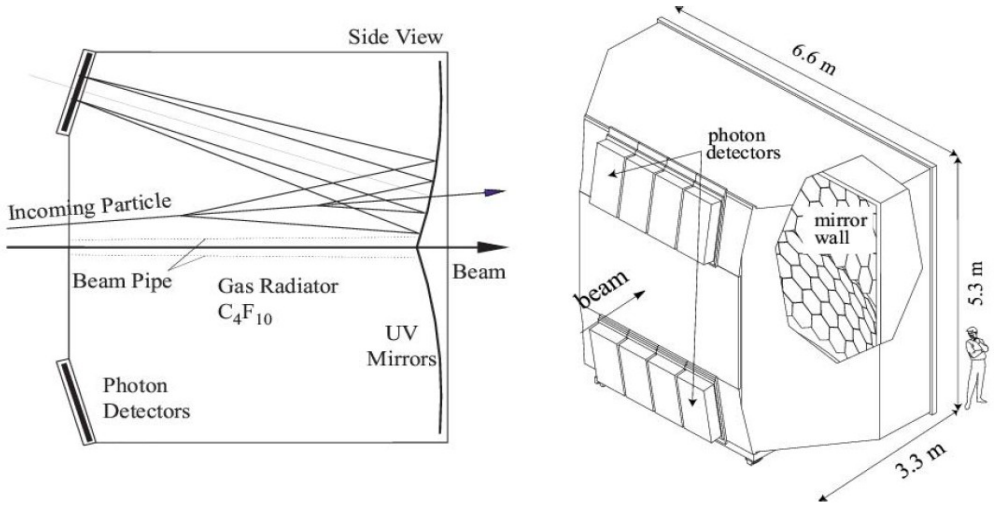

Figure 3.3: COMPASS RICH detector – scheme and artistic view

3.2.4 Muon identification

Muons are detected by Muon walls (MW1 in LAS and MW2 in SAS) which consists of several tracking planes and the muon filter i.e. absorber made of iron 60 cm thick in case of MW1 and concrete 2.5 m thick in case of MW2. The tracking planes are divided in two groups – one in front of the muon filter and one behind muon filter. The muon filters stops all other particles except muons, so if a track detected in front of muon filter continues behind the muon filter then the particle is a muon. Fig.3.4 shows the layout of MW1. The tracking is made by straw tubes in the case of MW1 and combination of straw tubes and MWPCs in the case of MW2.

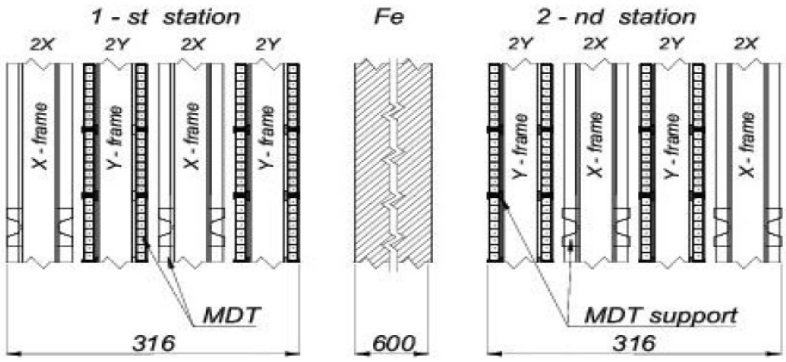

Figure 3.4: Muon wall 1

3.2.5 Trigger and Data Acquisiton sytem

Whole spectrometer contains several hodoscopes i.e. detector planes made of scintillators. Because of the fast response of the scintillators, the signals from them are used for trigger together with fast signals from calorimeters. The trigger electronics is located in separate barack inside the experimental hall. Trigger electronics (based on fast logic circuitry) then gives signal about which data to process further to the DAQ. The modularity of the trigger system allows for rather easy changes between different physics runs.

The COMPASS detectors have in total about 250 000 channels which need to be read out and processed. The average size of event is about 35 kB and trigger rate is about 50 kHz. (See [30].) The total volume of data produced per year is about 2 TB. This all poses high demands on DAQ. As the original system is becoming obsolete and spare parts are impossible to obtain it was decided to substantially update the DAQ and base it on FPGA[1] chips. The new system is supposed to be deployed already for Drell-Yan run in October 2014. (For details see e.g. [30].)

The COMPASS setup is now undergoing rather heavy upgrade to be ready for Drell-Yan data taking by the end of 2014. This includes modification of the polarized target, DAQ, new hadron absorber and improved muon tracking. For Details see e.g. [19].

1 Field-programmable gate array

3.3 Polarized Target

Polarized target is the key component of COMPASS experiment concerning the nucleon spin structure studies. It allows to measure the TMDs when transversely polarized and if it is longitudinally polarized it can be used to measure e.g. g_1 structure function or gluon polarization via open charm production i.e. gluon contribution to nucleon spin. Fig. 3.5 shows the target system layout.

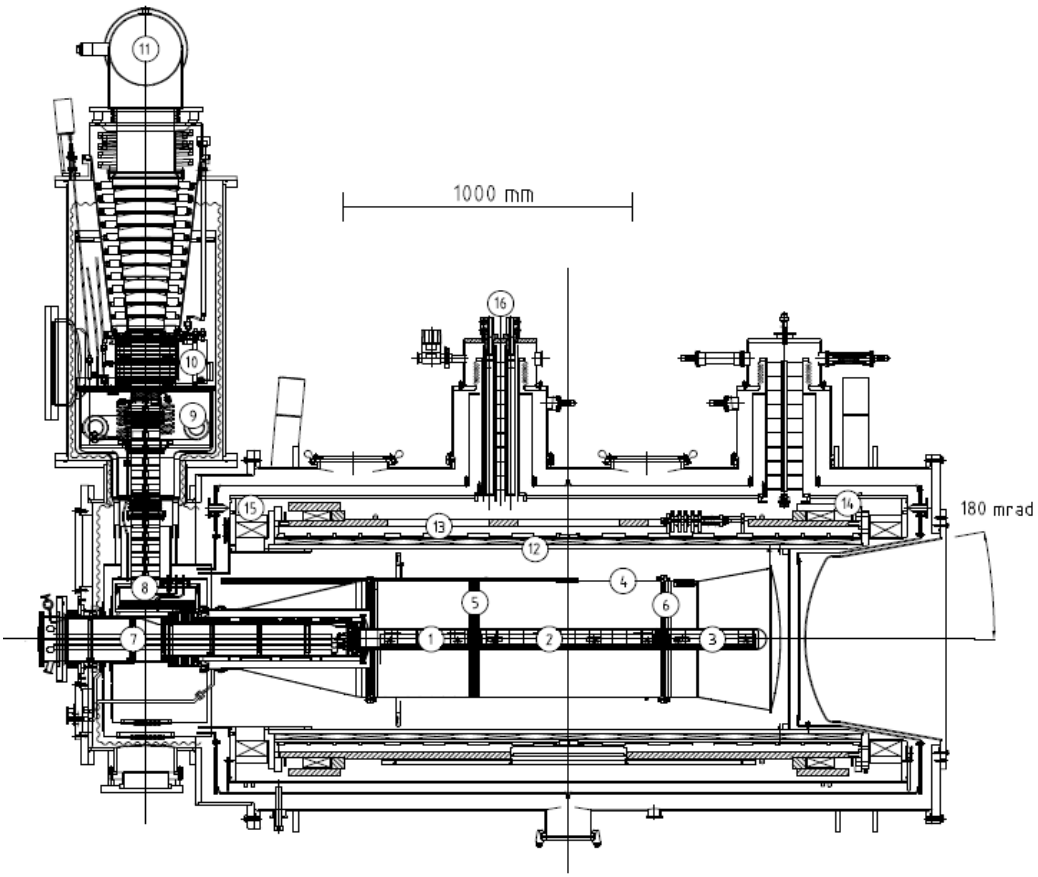

Figure 3.5: Side view of the COMPASS polarized target system: (1) upstream cell, (2) middle cell, (3) downstream cell, (4) microwave cavity, (5, 6) microwave stoppers, (7) target holder, (8) ^{3}He evaporator, (9) ^{4}He evaporator, (10) ^{4}He separator, (11) ^{3}He pumping port, (12) solenoid magnet, (13) correction coils, (14) dipole magnet, (15) solenoid compensation coil, (16) magnet current leads

As was shown in Chapter 2 for reaching high polarization and for sustaining it for a long period of time several things are needed – the high magnetic field, low enough temperature and the microwave system. We will now describe these components of the COMPASS PT in details.

3.3.1 Dilution refrigerator

COMPASS dilution refrigerator (DR) allows to cool down the target material down to temperature of about 70 mK with cooling power of 5 mW. Fig. 3.6 (taken from [31]) shows simplified schematics of COMPASS DR. Fig. 3.7 (also from [31]) shows temperature dependence of mixing chamber on ^{3}He flow at different cooling powers.

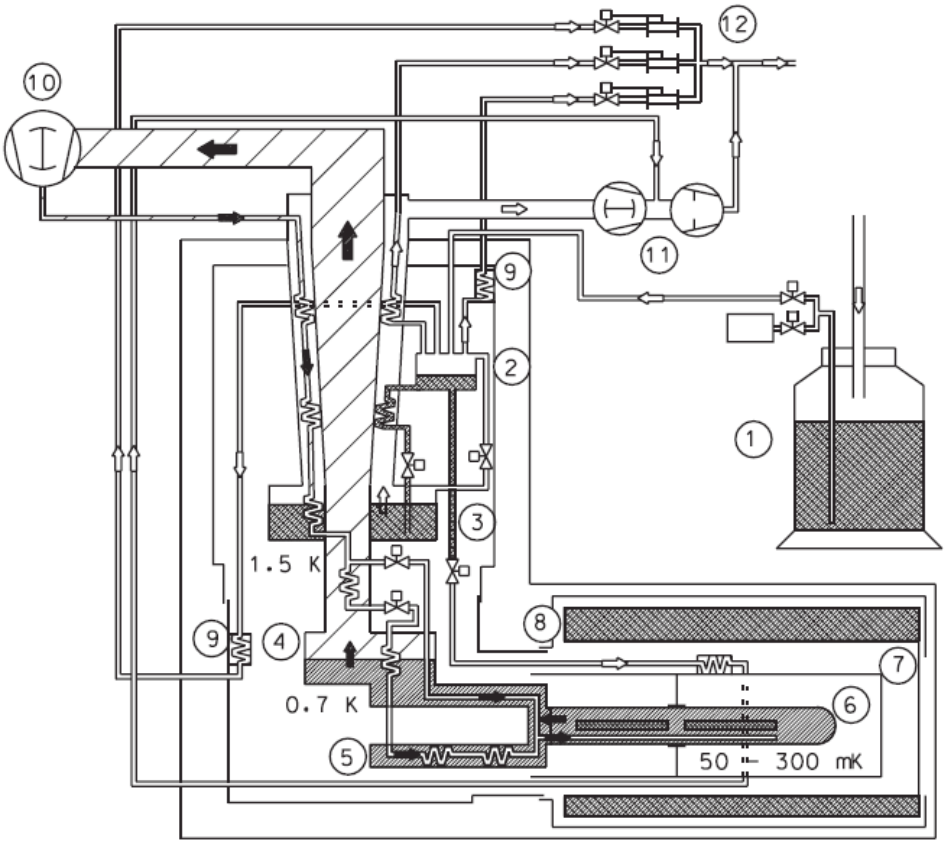

Figure 3.6: Schematics of COMPASS DR: (1) liquid ^{4}He buffer dewar (2000 l), (2) 4He gas/liquid separator, (3) 4He evaporator, (4) still, (5) main heat exchanger, (6) mixing chamber, (7) microwave cavity, (8) magnet liquid ^{4}He vessel, (9) thermal screen, (10) ^{3}He Root's pumps, (11) ^{4}He Root's and rotary pumps, (12) ^{4}He recovery line

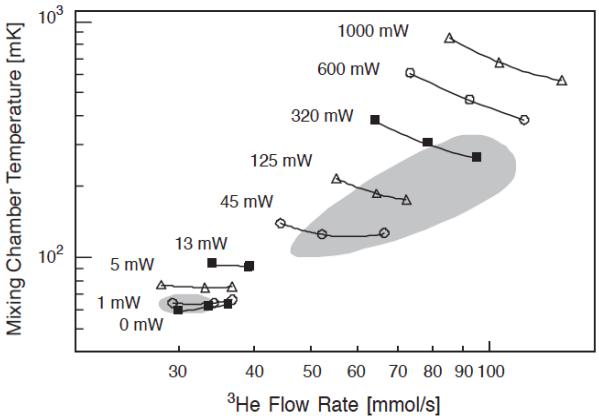

Figure 3.7: Dependence of the mixing chamber temperature on the ^{3}He flow. The shaded areas show regions where the DNP is performed (the larger one) and the frozen spin mode is maintained (smaller one)

The principle of how it works is as follows (see also [32]). Mixture of ^{3}He-^{4}He with specific molar concentration of ^{3}He is cooled down at about 1 K. Then as you can see in fig. 3.8 (which shows phase diagram of the mixture) the phase separation occur i.e. the phase rich in ^{3}He (concentrated phase) will be floating on the phase rich in ^{4}He (diluted phase) Then there is a capillary which ends in ^{4}He phase. Now if the helium atoms are forced to go trough boundary of the phases it will cause cooling as the ^{4}He is physical vacuum for ^{3}He atoms. There is clear similarity to classical evaporation of liquid which also causes cooling to occur. The space where the separate phases are being kept is called dilution (or mixing) chamber. Usually it is metalic container to which sample can be connected to be cooled down. The main difference at COMPASS PT refrigerator is that the material which is being cooled is placed directly into the dilution chamber making better thermal contact.

The dilution chamber itself has a diameter of approximately 7.5 cm and it is approximately 130 cm long which is enough to accommodate the three target cells of 4 cm diameter and length of 30 cm, 60 cm and 30 cm. The pumping of ^{3}He is obtained by 8 Pffeifer Root's blowers with total pumping speed of 13 500 m^3/h. The ^{3}He gas is purified by passing through zeolite filters and charcoal traps at LN_2 temperature and at room temperature. The working mixture consists of approximately 8800 l of ^{4}He gas and 1250 l ^{3}He gas (at normal temperature and pressure, according to latest helium inventory done in July 2013).

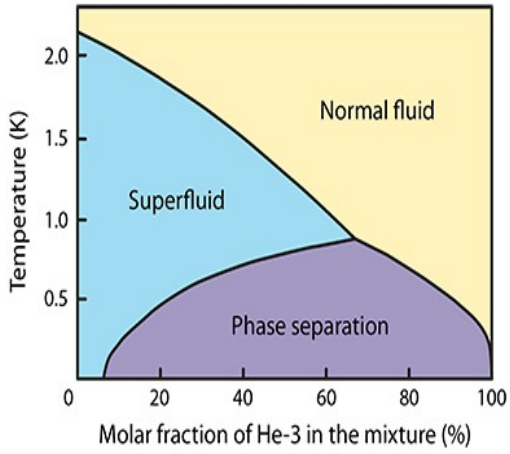

Figure 3.8: Phase diagram of ^{3}He – ^{4}He mixture

The cooling power can be deduced from enthalpy balance for the DR

$$\dot{n}_3[H_D(T_{mc})-H_C(T_{mc})]=\dot{n}_3[H_C(T_{ex})-H_C(T_{mc})]+\dot{Q}+\dot{Q}_{leak}+\dot{Q}_{\mu}\,, \qquad (3.1)$$

where T_{mc} is the mixing chamber ^{3}He outlet temperature, T_{ex} is the temperature at the ^{3}He inlet of the mixing chamber, H_D the is enthalpy of the diluted phase, H_C is the enthalpy of the concentrated phase, $\dot{Q}_{leak}$ is the heat leak, $\dot{Q}_{\mu}$ heating from muon beam, $\dot{Q}$ is the cooling power and $\dot{n}_3$ is ^{3}He flow rate. ^{4}He flow is not considered here. The cooling power can be then expressed from (3.1)

$$\dot{Q}=\dot{n}_3[H_D(T_{ex})-H_C(T_{mc})]-\dot{Q}_{leak}-\dot{Q}_{\mu}\,, \qquad (3.2)$$

where the $\dot{Q}_{leak}$ was estimated to be 4.2 mW and $\dot{Q}_{\mu}$ to be approximatelly 1mW in COMPASS case (see [26]). Even with this significant heat leak temperature about 60-70 mK is regularly achieved for the frozen spin mode (i.e. after the temperature is lowered down from the 300 mK used for DNP) to preserve the maximum polarization as long as possible.

The DR has about 36 thermometers for monitoring the temperatures and several pressure gauges and flow meters for monitoring both ^{3}He and ^{4}He flows. The temperature sensors are ruthenium oxide (RuO_2) and carbon Speer thermometers read out by four-wire AC resistance bridges with very low excitation and low noise analogue circuits to prevent parasitic heat input. For the precise temperature measurement at about 1 K (needed for TE calibration) the ^{3}He gas thermometer is used as it is primary thermometer for this temperatures according to ITS-90[2]

2 International temperature scale of 1990 [33]

temperature scale. The pressure is measured by high-precision capacitive gauge. The ^{3}He flow is regulated by motorized needle valves.

All the thermometers, pressure gauges and flowmeters were connected to computer running an application created in LabView system [34]. New software based on Unix system called ptread is foreseen for future runs and it is currently being developed. (See [35].)

The DR was helium leak tested at room temperature in 2013 with no leaks found. Needle valves were also tested because of suspected damage. No damage was found and the valves are working with almost no hysteresis. Example of test of one of the needle valves is shown in fig. 3.9.

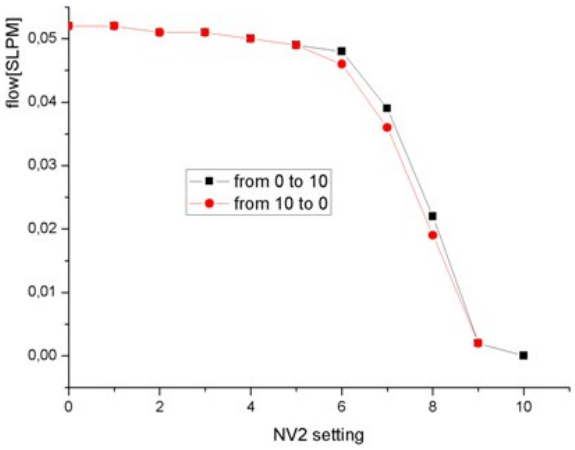

Figure 3.9: Needle valve testing: The black corresponds to opening of the valve whereas the red curve corresponds to closing of the valve.

3.3.2 Superconducting magnet

Another key component of the PT is the superconducting magnet. It consists of 2 main coils. The first one can create solenoidal field of 2.5 T and the second one can create dipole field of 0.6 T perpendicular to the solenoidal field. The main coils are supplemented by 10 trim coils and two correction coils to ensure homogenity of the magnetic field about 10^{-5} T. The magnetic field in the magnet can undergo so-called field rotation when the direction of the field is rotated by 180 ° without going through zero value i.e. without loss of polarization. This is done by simultaneous ramping up of the coil whose field we want to rotate and ramping up the second coil. This ensures non zero value of the field during whole procedure which lasts about 20

minutes. (Depending on the ramp up/ramp down speed.) The magnet provides angular acceptance of 180 mrad compared to the previously used SMC magnet which provided only 70 mrad.

Because of some operational problems during 2011 the magnet underwent significant modifications and new control and monitoring system was designed and built. As of March 2014 the magnet is undergoing final tests before reinstallation to COMPASS. Details will probably be published in near future.

3.3.3 Microwave system

The microwave system is responsible for irradiating the target material by microwave radiation at frequency about 70 GHz. (There are actually two frequencies for obtaining opposite polarization of the nuclei as was mentioned in Chapter 2.) The key element of this system is the microwave cavity which creates standing microwaves of given frequency inside its volume which is divided in three by two microwave stoppers each 5 cm long. The cavity is then simply a copper cylinder of 137 cm length and 40 cm diameter.. This setup allows to polarize each cell individually with different polarization. The three cells were usually polarized in such a way that the middle one had opposite polarization with respect to the outer two. The cavity is cooled by liquid helium to temperature about 4 K. Fig.3.10 shows typical polarization build-up of this three cell design target.

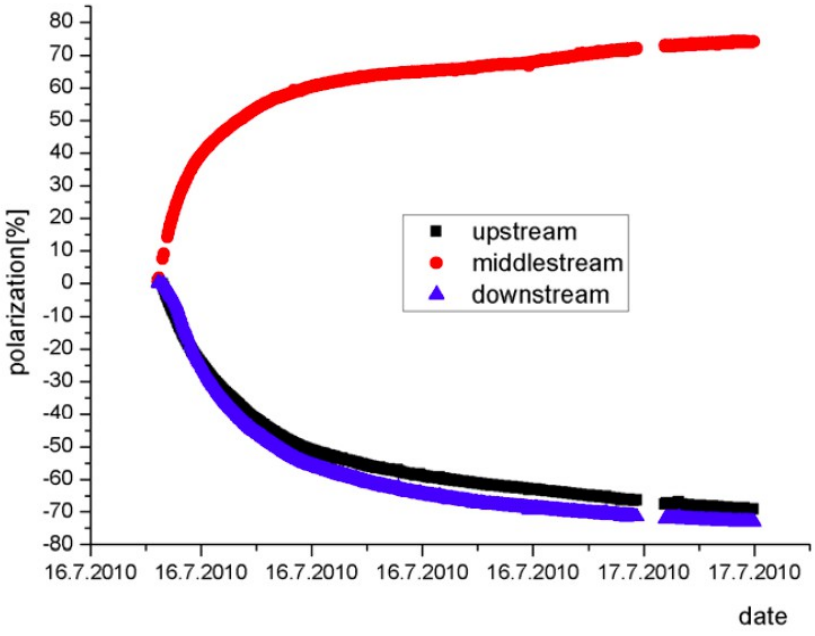

Figure 3.10: Polarization build-up on 16th July 2010

The cavity underwent modification during 2013 to accommodate for changes in the setup needed for 2014-2015 Drell-Yan run. Only two cells of 55 cm length will be used, so special adapter and new 20 cm long microwave stopper were produced.

The rest of the system consist mainly of two microwave generators (to enable opposite polarization buildup at the same time and thus build-up of polarization in the whole target at once). The generators are Extended Interaction Oscillator (EIO) tubes. They can be tuned coarsely in a range of about 2 GHz in the 70 GHz region by change of the cavity length and finely tuned by change of voltage of HV power supply. Two "home-made" microwave attenuators (as no commercial attenuators were available to withstand the MW power of about 15 W) are used for regulating the power of the microwaves. The MW frequency is monitored by two frequency counters. The MW generators are connected to MW cavity via 15 m long X-band waveguides.

3.3.4 NMR system

The target NMR system uses continuous wave NMR (see [32, 36]) based on 10 coils where 4 coils are for the middle cell and 3 each are for upstream and dowstream cell. Fig. 3.11 shows complete scheme of the NMR system. Design of the coils represents quite a challenge because of two counteracting demands on them.

The filling factor η (i.e. the space occupied by the material inside the coil) and the empty coil inductance L_0 should be as high as possible in order to produce strong signal. Also the sensitivity should be largest on the axis of the target where most of the scattering takes place. Thus embedding the coils in the material seems as the best solution. But this then lowers the dilution factor f, see the following section.

On the other hand too high inductance is dangerous due to possibility of producing superradiance (see [37]) during the field rotation which destroys the polarization. This can be suppressed by making the field inhomogeneous during the rotation and by making the coils low inductance.

For the future Drell-Yan run different number, placement and possibly design of the coils are foreseen. In total again 10 coils are foreseen, 5 for each cell. Two different placements are now in consideration. First is 4 coils outside the cell for measurement in longitudinal field and 1 inside the cell for measurement in transverse field. Other possibility is 3 coils outside and 2 inside.

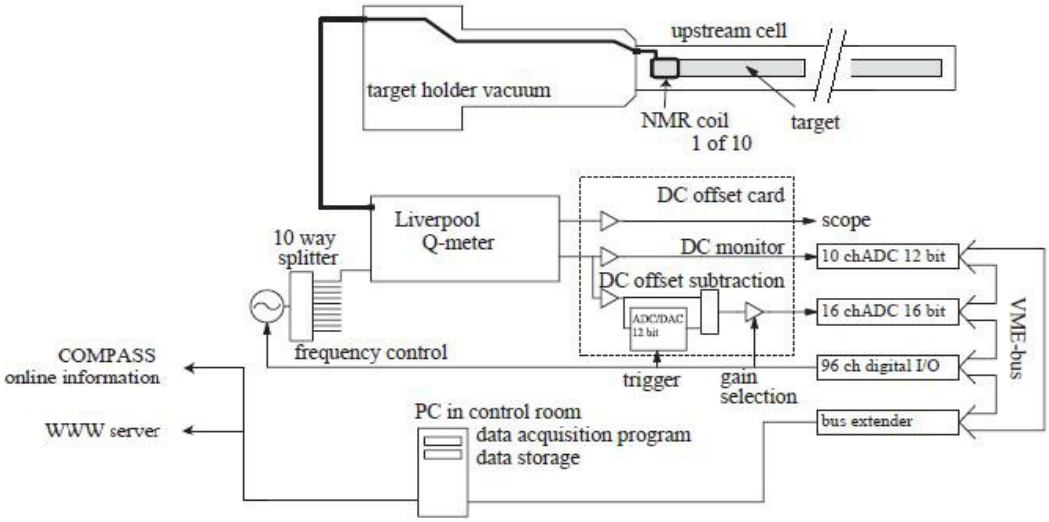

Figure 3.11: Scheme of PT NMR system

The coils are connected to the Q-meters, which amplify the signals and select the real part of the voltage. These are followed by Yale cards which subtract DC offset and further amplify the signals. The gain of the Yale cards can be set to 1, 207 and 334. The gain 207 is used for TE calibration. The final readout is then done by PC with custom written application in the LabView system.

3.3.5 Target material

The choice of the target material is crucial point in running the polarized target. To have the measuread asymmetries as high as possible the highest possible polarization is needed. To obtain largest possible statistics (to minimize statistical uncertainties) not only high intensity beam and as long target as possible is needed but also suitable target material. This can be expressed in quantitative way by the so called Figure of Merit F_{oM}.

$$F_{oM} = f^2 P^2 \rho F_p \,, \tag{3.3}$$

where F_p is so-called packing factor, ρ is the target material density, P is maximum polarization of the material and f is so-called dilution factor, which describes the fractions of events on polarized nuclei with respect to the unpolarized ones. It is defined as

$$f = \left(1 + \frac{n_A \sigma_A}{n_p \sigma_p}\right)^{-1} , \tag{3.4}$$

where σ_A is cross-section for unpolarized nucleus, σ_p is cross-section for polarized

nucleus and n_A and n_p are molar densities of the respective nuclei. Fig. 3.12 shows the dependence of f on kinematic variable x for three different target materials.

Another important thing is that if one intents to measure on neutron target the only reasonable choice is deuterated material. In past COMPASS has used deuterated lithium ^{6}LiD and ammonia NH_3. The SMC collaboration used also deuterated butanol. Al these materials differ in maximum achievable polarization, relaxation time, the way of creation of the paramagnetic centres for DNP and dilution factor. We will now give some information on the first two of them as they are the only ones used in COMPASS so far. More detail can be found in e.g. [25].

Ammonia

The NH_2 radicals needed for DNP are produced by irradiation at low temperature with 20 MeV electrons at Bonn University linac. Liquid ammonia droplets are dropped into liquid nitrogen which leads in formation of small balls with approximately 4 mm diameter. The maximum polarization achievable is over 95 % where about 80 % to 90 % was usually reached at COMPASS experiment during 2010 and 2011. The average value of dilution factor f is 0.15. The NH_3 molecule has triangular configuration of the protons which results in asymmetric lineshape at high polarizations.

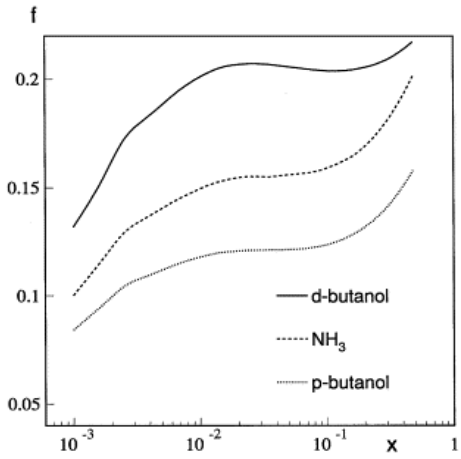

Figure 3.12: Dilution factor for deuterated butanol, ammonia and butanol

Deuterated lithium

The ^{6}LiD has not been used in 2010 and 2011 runs. The maximum polarization reachable is about 55 % using the frequency modulation i.e. modulation of the MW signal by 30 MHz triangular waveform leads to considerable increase in polarization. The average dilution factor is 0.22. For more details see e.g. [37].

4. Polarization measurements during COMPASS runs 2010 and 2011

4.1 Principles of the measurement

Consider ensemble of nuclear spins with magnetic moment μ. The macroscopic magnetization is then given

$$M = \mu NP \text{ and also } M = \chi_0 B \,, \tag{4.1}$$

where N is density of the magnetic moments, P is polarization, χ_0 is static susceptibility and B is static external field. If one introduces time dependent external field the susceptibility becomes dynamical one

$$\chi(\omega) = \chi'(\omega) - i\chi''(\omega) \,, \tag{4.2}$$

where χ' is the dispersive part of the susceptibility and χ'' is the absorptive part of susceptibility. The famous Kramers-Kronig relations which connect the dispersive and absorptive parts imply

$$\chi_0 = \chi'(0) = \frac{2}{\pi} \wp \int_0^\infty \frac{\chi''(\omega')}{\omega'} d\omega' \,, \tag{4.3}$$

where $\wp$ denotes the principal value of the integral. Using (4.1) one gets the expression for the polarization

$$P = \frac{\chi_0 B}{\mu N} = \frac{2}{\pi \hbar \gamma^2 I N} \wp \int_0^\infty \chi''(\omega') \frac{\omega_0}{\omega} d\omega \,, \tag{4.4}$$

where ω_0 is the Larmor frequency of the nuclei.

As the NMR line is very narrow (i.e. the absorptive part is non-zero only in narrow range of frequency, at COMPASS typically about 400 kHz) the ratio ω_0/ω is close to one i.e. the polarization is proportional to integral from absorptive part of the susceptibility.

If a coil is embedded into a material with susceptibility χ then the inductance L_0 of the coil changes

$$L(\omega) = L_0(1 + \eta\chi(\omega)) \,, \tag{4.5}$$

where η is the filling factor which describes how large fraction of the coil volume is filled by the material. Now the coil impedance

$$Z_c = R_c + i\omega L(\omega) \tag{4.6}$$

can be measured using the Q-meter. Its scheme is shown in fig.4.1. The Q-meter output is complex voltage *V(χ, ω)* of which the real part is selected by phase-sensitive detector. The Q-meter is tuned so that the minimal voltage is for Larmor frequency ω_0. The RF synthesizer provides voltage which is swept around the ω_0.

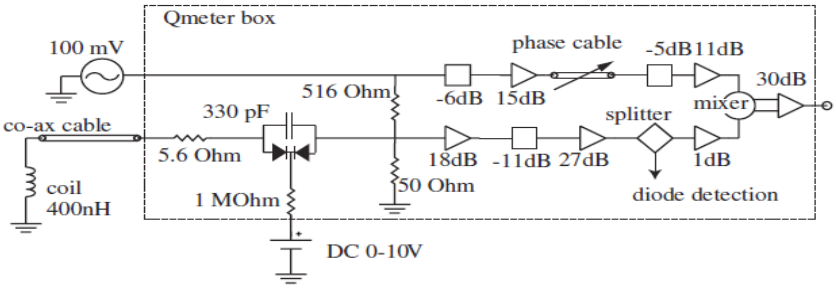

Figure 4.1: Q-meter schematics

The measurement itself proceeds in two steps. Firstly the magnetic field is lowered little bit from its nominal value which causes the nuclei to get off-resonance and the so-called baseline (or Q-curve) *V(ω,χ''=0)* is taken. Then the NMR signal is taken at the nominal field. Then the subtracted signal

$$S \equiv \Re[V(\omega,\chi)] - \Re[V(\omega,\chi''=0)] \tag{4.6}$$

is obtained, where $\Re$ denotes real part. It can be show by circuit analysis (see [25]) that $S \propto \chi''(\omega)$ which yields

$$P = C\int S(\omega)\,d\omega\,. \tag{4.7}$$

The polarization of a system at thermal equilibrium (TE) is given by Brillouin function [38]

$$P(x) = \frac{2I+1}{2I}\tanh\left(\frac{2I+1}{2I}x\right) - \frac{1}{2I}\coth\left(\frac{1}{2I}x\right), \quad x = \frac{\gamma\hbar IB}{k_B T}\,, \tag{4.8}$$

which simplifies to

$$P(x) = \tanh(x) \tag{4.9}$$

for spin ½. This allows for determination of the constant C in (4.7) if the NMR signals are measured for both TE and enhanced polarization situation.

4.2 Data processing and TE calibration for 2010 and 2011

As was shown in the previous section the polarization is proportional to the area of the NMR signal. The constant of proportionality is obtained by so-called thermal

equilibrium (TE) method which is based on the fact that the polarization can be directly calculated for material where nuclear system is in thermal equilibrium with the lattice. From that the calibration constant can be obtained which can be used even for dynamically polarized system which is no longer in TE.

At COMPASS the TE calibration is done for several (typically 3 or 4) different temperatures around 1 K (which is reasonable compromise between spin-lattice relaxation time and signal size). The TE calibration is performed twice at the beginning of the physics run. Firstly TE signals are taken without target material loaded. This is for determining any possible background from protons in target holder etc. Secondly TE signals are taken with target material loaded. The time period for each temperature is of order of about 10 hours. One signal is taken every 3 minutes and for each coil. The temperature during TE calibration is measured primarily by ^{3}He vapour pressure thermometer and is backed up by ruthenium oxide thermometers which are commonly used for the monitoring of the target DR during physics run as mentioned in section 3.3.

As was already mentioned the TE polarization is very small (0.0025 for ^{1}H in ammonia at 2.5 T field and 1 K temperature) and the signals need to be amplified significantly and they also suffer from significant noise. As the result of this the frequency range for fitting the residual baseline after Q-curve subtraction is not straightforward to determine. Different ranges gives different integrated areas as the final signal is slightly different each time. To cope with that easy method based on simple statistics is applied.

The NMR signal is taken in range of 600 kHz. From this range central part around the resonance peak is excluded for the residual baseline fitting. The exclusion starts with windows of 200 kHz and proceeds in 20 kHz steps up to 440 kHz. Then all the signals with subtracted residual baseline are integrated and resulting areas are averaged. This is repeated for all data for given TE period when the temperature is stable enough. (Stability of temperature required is better than 20 mK.) As the argument of hyperbolic tangent in formula (4.9) is (in COMPASS case) of order of about 10^{-3} it is safe to use Taylor expasion to the first order which basically gives the famous Curie law and fit the obtained values of area against inverse temperature. Now using formula (4.7) for TE polarization at 1 K one obtains the constant of proportionality for determining the polarization. (One needs to take into account the

gain of the amplifier which makes the area seemingly larger and to subctract from that also the value obtained from empty target TE calibration to get pure target material proton calibration.) Fig.4.2 and fig.4.3 show typical Curie fit for coil number 3 for emty target and loaded target calibration during 2010 and fig.4.4 shows loaded Curie fit for the same coil in 2011. Tab.4.1 shows TE calibration temperatures for 2010 and 2011 without uncertainties which are discussed in section 4.5. Fig.4.5 then shows typical NMR signals.

Loaded 2010	Empty 2010	June 2011	November 2011	November 2011 empty
1.500	1.560	1.471	1.465	1.502
1.293	1.349	1.306	1.260	1.275
1.172	1.096	1.143	0.993	1.012
	1.073			

Table 4.1: TE calibration temperatures, all corresponds to values meassured by ^{3}He vapour pressure thermometer except November 2011 loaded TE calibration when the ^{3}He bulb was blocked and data could not be used, uncertainties are discussed latter on

It should be also mentioned that during the analysis several of the signals were thrown away because of the readout errors and in total there were about 10 000 signals processed for both years together.

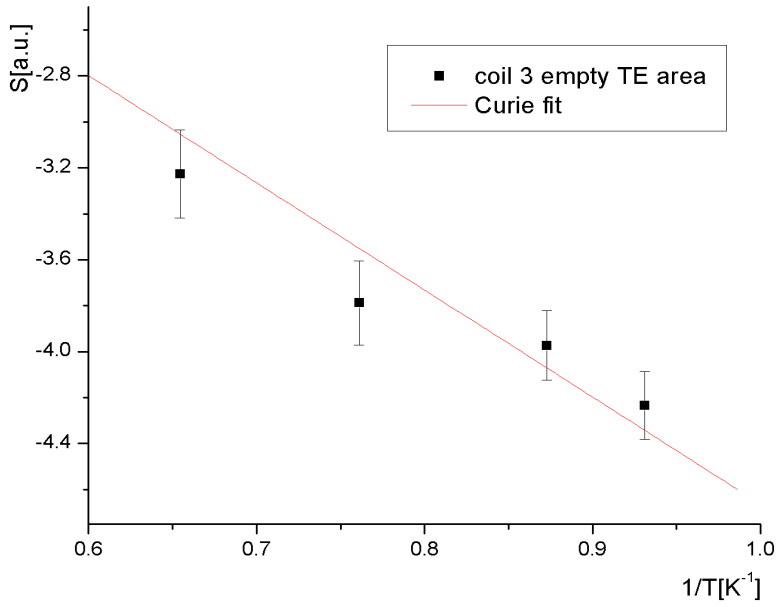

Figure 4.2: Empty TE calibration for coil 3 run 2010

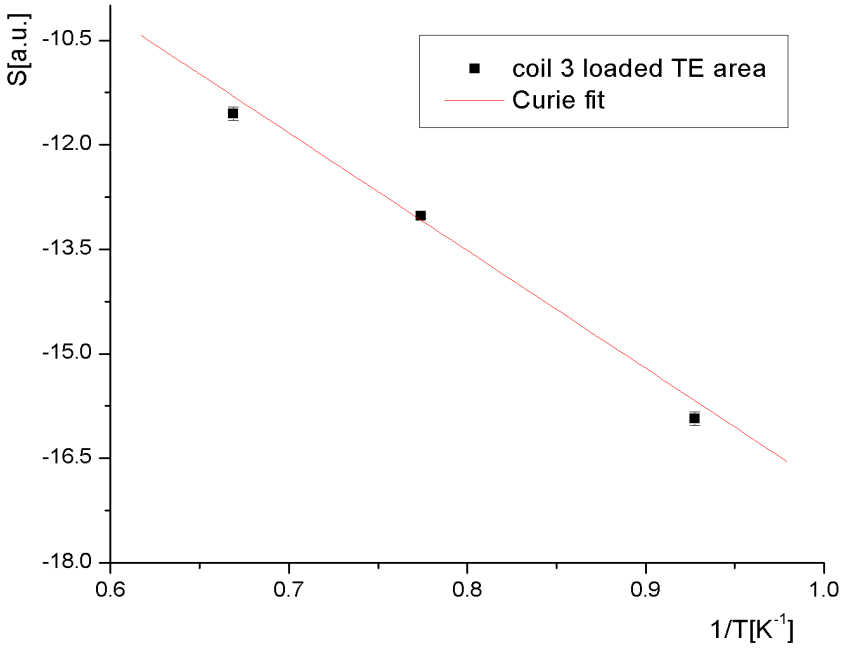

Figure 4.3: Loaded TE calibration for coil 3 run 2010

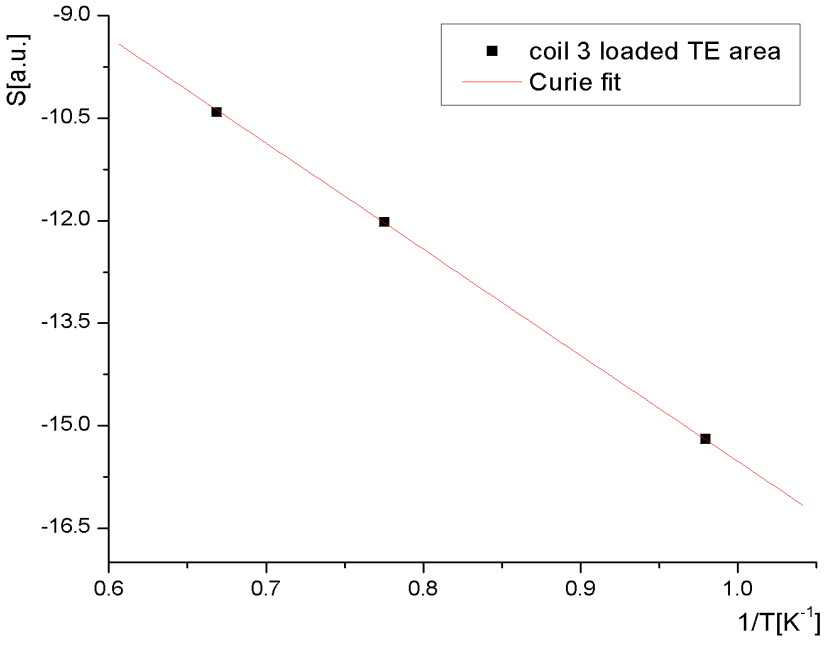

Figure 4.3: Loaded TE calibration for coil 3 run 2011

Finaly the result is exactly 10 calibration constants which allows to determine polarization in each target cell for whole physics run by simply integrating area of NMR signal for enhanced polarization. Tab.4.2 shows calibration results for 2010

and tab.4.3 shows results for 2011. All uncertainties are statistical only, systematics are discussed in following sections.

Coil No.	Empty	Loaded	NH_3	Gain	Calibration Constant
1	-3.73±0.16	-6.83±0.11	-3.1±0.2	213.8	-17.5±1.1
2	-4.37±0.15	-22.37±0.30	-18.0±0.4	213.8	-3.01±0.06
3	-4.59±0.07	-16.90±0.10	-12.3±0.1	213.2	-4.39±0.05
4	-5.49±0.16	-20.40±0.21	-14.9±0.3	214.4	-3.64±0.06
5	-5.23±0.10	-15.09±0.18	-9.9±0.2	211.3	-5.43±0.11
6	-4.29±0.11	-19.25±0.08	-15.0±0.1	213.7	-3.62±0.03
7	-2.70±0.10	-17.34±0.14	-14.6±0.2	217.1	-3.76±0.04
8	-3.62±0.12	-16.86±0.14	-13.2±0.2	214.4	-4.10±0.06
9	-4.58±0.08	-15.36±0.17	-10.7±0.2	215.4	-5.06±0.09
10	-6.46±0.21	-25.78±0.20	-19.3±0.3	212.6	-2.79±0.04

Table 4.2: TE calibration for 2010, the empty, loaded and NH3 columns corresponds to Curie constants[3] for calibration with empty and loaded target and subtracted result corresponding to pure ammonia signal. The gain corresponds to gain of the amplifier used during calibration

Coil No.	Empty	Loaded	NH_3	Gain	Calibration Constant
1	-3.87±0.03	-16.17±0.07	-12.3±0.1	213.4	-4.35±0.03
2	-4.22±0.02	-19.9±0.1	-15.7±0.1	213.0	-3.47±0.01
3	-4.88±0.03	-15.58±0.05	-10.71±0.04	212.8	-4.94±0.03
4	-5.84±0.03	-21.5±0.1	-15.64±0.08	214.0	-3.48±0.02
5	-5.38±0.03	-15.9±0.1	-10.51±0.05	210.7	-4.87±0.04
6	-4.25±0.05	-17.45±0.05	-13.2±0.1	213.0	-4.10±0.01
7	-2.67±0.02	-16.57±0.07	-13.9±0.1	216.1	-3.86±0.02
8	-3.51±0.05	-17.41±0.08	-13.9±0.1	213.5	-3.91±0.02
9	-4.58±0.04	-17.18±0.06	-12.61±0.05	212.0	-4.22±0.02
10	-6.24±0.14	-24.5±0.2	-18.3±0.3	211.9	-2.92±0.05

Table 4.3: TE calibration for 2011, the empty, loaded and NH3 columns corresponds to Curie constantsfor calibration with empty and loaded target and subtracted result corresponding to pure ammonia signal. The gain corresponds to gain of the amplifier used during calibration

3 i.e. result of Curie fit for NMR signal areas, not Curie constant is the strict sense of Curie law for susceptibility

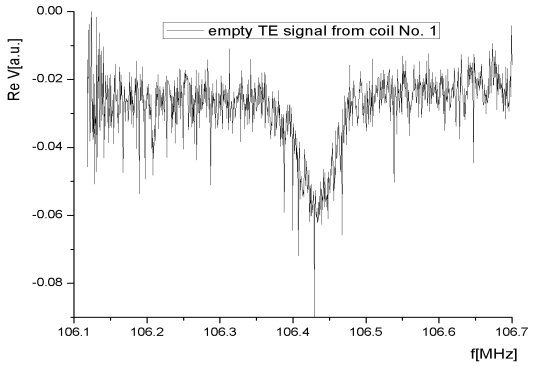

a)

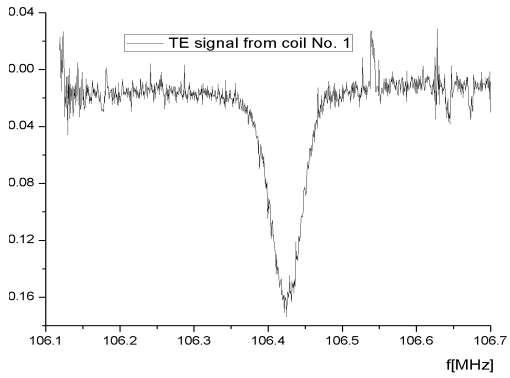

b)

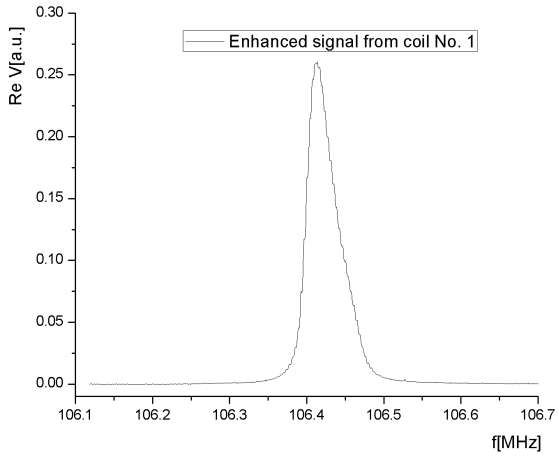

c)

Figure 4.5: NMR signals for coil 1: a) empty TE signal, b) loaded TE signal and c) enhanced polarization signal

4.3 Average polarization for 2010 and 2011

The final average polarization for each cell is usually given for each run and is stored in COMPASS database to be accessible for physics data analysis. Here we present only average polarization for whole year 2010 and 2011. The polarization for each cell is average weighted by each coil uncertainty. Overall polarization for whole year is obtained as average weighted by number of events in each cell.

Cell	Polarization 2010	stat[%]	sys[%]	Polarization 2011	stat[%]	sys[%]
up	0.789	2.2	3.7	0.836	2.0	3.7
middle	0.796	1.2	3.5	0.863	1.7	3.4
down	0.798	1.2	3.2	0.827	1.8	3.1

Table 4.4 Average polarization for 2010 and 2011 together with their uncertainities

4.4 Comparison and comments on 2010 and 2011 results

As can be seen the maximum polarization value obtained in 2010 and 2011 differs quite significantly. There was virtually no change in the target system during these two years and the explanation is that here was more time available for polarization buildup in 2011 than in 2010.

Another significant difference is between calibration constant for coil number 1 in the upstream cell. The value from 2010 is much higher (in absolute value) than 2011. This is given by much smaller NMR signal detected by the coil. It was found after target material unloading that the material was badly loaded in the upstream coil and there was rather lower quantity of the material in the volume of the first coil.

MW leak test was performed at the end of 2010 and again in June 2011. Only the middle cell was polarized and polarization in all cells was measured. The results were 1.7 % , 75.2 % and 5.1 %[4] for upstream, middlestream and downstream cell respectively. This shows slight MW leak between cells. It agrees with final polarization results for 2011 i.e. maximum polarization in middlestream cell and lower in adjacent cells. However the difference is not visible in 2010.

The polarization of ^{14}N was not measured during 2010 and 2011 as this poses some difficulties with COMPASS target setup. However assuming equal spin temperature between nitrogen and protons in ammonia molecule the ^{14}N polarization can be calculated. As was already mentioned the assumption of equal spin temperature was verified by the SMC in [25]. The ^{15}N is not considered here as its natural abundance is only 0.37 %.The results for 2011 are shown in tab.4.5.

cell	2010	2011
upstream	0.082	0.116
middlestream	0.089	0.124
downstream	0.090	0.113

Table 4.5: ^{14}N polarization determined from the assumption of equal spin temperature, uncertainties are not determined as the polarization value serves only for illustration

4 It should be noted that two ways of presenting polarization values are used. That giving the absolute number e.g. 0.85 which correspond to 85 %, which style is used here

The relaxation rates and relaxation times were also determined for both years. These are quite different as the magnetic field was different i.e. transverse field of 0.6 T in 2010 and 2.5 T in 2011. The average relaxation rate for 2010 was about 0.35 % per day and 0.12 % per day in 2011. The relaxation times were about 4 500 h in 2010 and about 11 000 h or larger in 2011.

All these results are also summarized in [39], [40] and partially in [41].

4.5 Systematic uncertainties

The question of systematic uncertainties is rather difficult. Only general overview and the most significant sources of systematics will be given in this section. Comprehensive study of all possible effects can be found in paper by the SMC collaboration [25]. Most of the systematics are treated rather conservatively at COMPASS with respect to detailed studies performed by the SMC.

4.5.1 Temperature measurement

Temperature measurement is one of the main sources of systematic uncertanity for TE calibration and consequently whole polarization determination. One needs to ensure as stable temperature during the calibration as possible and to measure it with great accuracy.

As was already mentioned the precision of the temperature measurement is ensured by the use of ^{3}He vapour pressure thermometer. This brings systematics (whose sources are the inherent ITS90 scale accuracy, baratron pressure measurement and uncertainty of voltmeter used for reading the baratron) at the order of about 2.5 mK. ^{3}He thermometer brings of course some operational difficulties which can be illustrated on 2011 data. During TE calibration period of 9th November to 12th November the tube of the thermometer was partially blocked and only the values obtained by ruthenium oxide resistive thermometers could be used and which needed correction due to magnetic field of the target solenoid. This brought the uncertainty up 15 mK. (This of course does not concern 2010 measurement when ^{3}He thermometer operated with no problems.) The instability of temperature brought statistical uncertainity of the temperature measurement in the range of 1.6 mK up to 15 mK and in two cases up to 39 mK (see [39] and [40]). The total uncertainity brought to the polarization values is about 2.5 %.

4.5.2 Other systematics

We now briefly discuss other main contributions to the systematic uncertanities.

Magnetic field polarity

If was found already by the SMC collaboration in [25] that the magnetic field orientation changes the resulting NMR area. The reason is not completely clear, it can be however quantified. The TE calibration is not affected as it is taken only with one field polarity. The correction to the polarization is about few percent with total uncertainty about 1 %.

Non-linearity of Q-meter circuit

Due to Q-meter non-linearity the NMR peak frequency shifts with larger polarization values (i.e. larger amplitude of the signal). The shift is about 30 kHz. This brings overall uncertainty to the polarization about 1 %.

NMR signal integration and residual baseline

The noise on TE signal bring some uncertainty to the integrated area. Generally the residual baseline fit and subtraction contribute as well as only only linear fit is used for determination of the residual baseline. The overall contribution the uncertainty is then about 0.6 %.

For more detailed discussion see COMPASS Elog [39] and COMPASS note [40].

Conclusion

In the presented thesis we demonstrated the importance of the large polarized target for the nucleon spin structure studies using Deep inelastic scattering. The possibility to measure the TMDs using the polarized target (as a key experimental part) and SIDIS was demonstrated. The future single-polarized Drell-Yan measurement using the COMPASS polarized target was mentioned with accent given to much needed universality test i.e. change of sign of T-odd TMDs when measured in SIDIS and Drell-Yan.

The COMPASS experiment at CERN was described and its main results in context of nucleon spin structure studies were presented. Extensive overview of COMPASS polarized target was presented along with remarks on its performance during runs 2010 and 2011 and the choice of the target material was briefly discussed. Some remarks about modifications needed for the future Drell-Yan programme were also presented along with the results on the tests of dilution refrigerator needle valves during 2013.

Finally the TE calibration procedure was described and the TE calibration neeeded for the target polarization measurement was carried out together with determination of the average polarization during both 2010 and 2011 and was discussed in much details. The polarization results form basis of several important physics measurement, namely Collins and Sivers asymmetry measured on transversely polarized target in 2010 and A_1 asymmetry measured on longitudinally polarized target in 2011. The average polarization was determined to be about 0.8 during 2010 and about 0.85 during 2011 with statistical uncertainty about 2 % and systematic uncertainty about 3.5 %, where main contribution comes from temperature measurement uncertainty. The difference in average polarization between years is mainly due the fact that there was less time available for polarization build-ip in 2010 than in 2011. Using the assumption of equal spin temperature the ^{14}N nitrogen polarization was determined to be about 0.09 in 2010 and 0.11 in 2011. Relaxation times were determined to be at the order of 5 000 hours for 2010 and more than 10 000 hours for 2011. These allow for long physics measurement periods needed in the particle physics experiment.

Bibliography

[1] Chýla J.: Quarks, partons and Quantum Chromodynamics, Praha, 2004, available at http://www-ucjf.troja.mff.cuni.cz/new/wp-content/uploads/2014/02/text.pdf

[2] Devenish D., Cooper A.,Deep inelastic scattering, Oxford University Press, 2011

[3] Itzykson C., Zuber J.-B.: Quantum field theory, McGraw-Hill Inc., 1980

[4] Klíma J., Velický B.: Kvantová mechanika II, Karolinum, 2005

[5] Bjorken J.D., Phys. Rev 179 (1969), 1547

[6] Targett-Adams C., On behalf of Zeus and H1, arxiv:hep-ex/0507024v1 (2005)

[7] Bjorken J.D., Paschos E.A. Phys. Rev. 185 (1969), 1975

[8] Gross D.J., Wilczek F., PRL 30 (26) ,1343-1346

[9] Politzer H.D., PRL 30 (26), 1346-1349

[10] Gross D.J., Wilczek F., Phys. Rev. D 8 (1973), 3633

[11] Martin A.D. et al. Eur. Phys. J. C63 (2009) 189-285

[12] Barone, V. et al. Phys. Rept. 359 (2002) 1.

[13] Jaffe R.L., Manohar A., Nucl. Phys. B 337 (1990), 509

[14] Alekseev M. et al., Phys. Lett. B 693 (2010), 227-235

[15] Ashman J. et al., Nucl. Phys. B 328 (1989) 1.

[16] Baccheta A. et al. JHEP 0702 (2007), 93

[17] Diehl M., Sapeta S., Eur. Phys. J. C41 (2005), 515-533

[18] Gautheron F. et al.: COMPASS-II Proposal, 2010, CERN, Geneva

[19] Matoušek J.: Studies of Drell-Yan process at Compass experiment, Diploma thesis MFF UK, Praha, 2013, available at http://physics.mff.cuni.cz/kfnt/cern/files/matousek-diploma_thesis.pdf

[20] Andrieux V. et al.: COMPASS A_1 release note, 2012, available at http://wwwcompass.cern.ch/compass/results/2012/september_A1_proton/release_note.pdf

[21] Collins J., Nucl. Phys. B 396 (1993), 161-182

[22] Adolph C. et al.: COMPASS Collins and Sivers asymmetries, 2011, available at

http://wwwcompass.cern.ch/compass/results/2011/august_transv_1h/release_note.pdf

[23] Abragam A., Goldman M., Rep. Prog. Phys. 41 (1978), 395

[24] de boer W., Dynamic orientation of nuclei at low temperatures, CERN, 1974

[25] Adams D. et al., NIMA 437 (1999) 23-67

[26] Abbon et al.: Compass experiment at CERN

[27] Charpak G. et al., Nucl. Intrum. Methods Phys. Res. A 376 (1996), 29

[28] Sauli F. et al., Nucl. Intrum. Methods Phys. Res. A 386 (1997), 531

[29] Breskin A. et al., Nucl. Intrum. Methods Phys. Res. A 535 (2004), 303

[30] Bodlak M. et al., JINST 8 (2013) C02009

[31] Doshita N. et al., NIMA 526 (2004), 138-143

[32] Skrbek L. et al.: Fyzika nízkých teplot, MatFyz Press, 2011

[33] http://www.its-90.com

[34] http://www.ni.com/labview/

[35] https://git.cern.ch/web/?p=ptread.git

[36] Slichter C.P.: Principles of magnetic resonance, Springer Verlag, 2008

[37] J. Ball et al.: First result on the large COMPASS 6LiD polarized target, NIMA 498 (2003) 101-111

[38] Kittel Ch.: Introduction to solid state physics, Wiley, 2004

[39] http://wwwcompass.cern.ch/elog/target_polar/186

[40] Koivuniemi J., Pesek M. et al.: COMPASS Note 2013-7, CERN, Geneva, available at http://wwwcompass.cern.ch/compass/notes/2013-7/2013-7.pdf

[41] Pešek M.: Low temperature proton polarized target for nucleon structure studies at COMPASS, Bachelor thesis, MFF UK, Praha, 2012, available at http://wwwcompass.cern.ch/compass/publications/theses/2012_bac_pesek.pdf

List of Tables

List of Abbreviations

CERN – European organization for nuclear research

COMPASS – Common muon and proton apparatus for structure and spectroscopy

χPT – Chiral perturbation theory

DAQ - Data acquisition

DC – Drift chamber

DIS – Deep inelastic scattering

DNP – Dynamic nuclear polarization

DR – Dilution refrigerator

DY – Drell-Yan

GEM – Gaseous electron multiplier

MWPC – Multiwire proportional chamber

NMR – Nuclear magnetic resonance

PDF – Parton distribution function

PT- Polarized target

QED – Quantum electrodynamics

QCD – Quantum chromodynamics

RICH – Ring imaging Cherenkov

SIDIS – Semi-inclusive deep inelastic scattering

SMC – Spin muon collaboration

SPS – Super proton synchrotron

ThGEM – Thick gaseous electron multiplier

TMD – Transverse momentum dependent parton distribution function